# Resonant tunneling through ultrasmall quantum dots: Zero-bias anomalies, magnetic-field dependence, and boson-assisted transport

Jürgen König, Jörg Schmid, and Herbert Schoeller
*Institut für Theoretische Festkörperphysik, Universität Karlsruhe, 76128 Karlsruhe, Germany*

Gerd Schön
*Institut für Theoretische Festkörperphysik, Universität Karlsruhe, 76128 Karlsruhe, Germany*
*and Department of Technical Physics, Helsinki University of Technology, 02150 Espoo, Finland*
(Received 21 June 1996; revised manuscript received 29 August 1996)

We study resonant tunneling through a single-level quantum dot in the presence of strong Coulomb repulsion beyond the perturbative regime. The level is either spin degenerate or can be split by a magnetic field. Furthermore we discuss the influence of a bosonic environment. Using a real-time diagrammatic formulation, we calculate transition rates, the spectral density, and the nonlinear *I-V* characteristic. The spectral density shows a multiplet of Kondo peaks split by the transport voltage and the boson frequencies and shifted by the magnetic field. This leads to zero-bias anomalies in the differential conductance, which agree well with recent experimental results for the electron transport through single-charge traps. Furthermore, we predict that the sign of the zero-bias anomaly depends on the level position relative to the Fermi level of the leads. [S0163-1829(96)03047-0]

## I. INTRODUCTION

The experimental study of tunneling through zero-dimensional states in quantum dots with high charging energies has received considerable interest recently.[1–7] Theoretical studies cover the classical regime (high temperatures[8–12]) as well as the quantum-mechanical regime (low temperatures[13–23]). In the latter case, Coulomb blockade and resonant-tunneling phenomena together with nonequilibrium generalizations of the Kondo effect are expected to occur. This leads to zero-bias anomalies in the differential conductance, which have been observed recently by Ralph and Buhrman.[24] In this article, we present a real-time diagrammatic approach to describe resonant tunneling at low temperatures and compare our results to the latter experiment.

The experiments for Coulomb blockade phenomena in zero-dimensional systems are usually performed in double-barrier resonant-tunneling structures,[2,3] split-gate quantum-dot devices,[4–6] quantum point contacts with single-charge trap states,[24] and quite recently also in ultrasmall metallic tunnel junctions[7] with Al particles of diameter below 10 nm. In the latter experiment, the level spacing is of order 0.5 meV which is comparable to the Coulomb charging energy in usual quantum dots. Therefore, the quantum dot is described by the nonequilibrium Anderson model where the energy level $\epsilon_\sigma$ (with spin label $\sigma$) is coupled via tunneling barriers to two electron reservoirs with different electrochemical potentials $\mu_L$ and $\mu_R$. The charging energy is described by a strong on-site Coulomb repulsion $U$ that suppresses double occupancy of the dot level. In equilibrium, it is well known from the theory of strongly correlated fermions[25] that the spectral density of the dot can exhibit a Kondo resonance at the Fermi level. It occurs for a low-lying level $\epsilon_\sigma - \mu_{L,R} < -\Gamma$ and weak Zeeman splitting $|\epsilon_\sigma - \epsilon_{\bar{\sigma}}| < \Gamma$, where $\Gamma/2$ is the level width in the noninteracting case, and provided that temperature is lower than the Kondo temperature[25,26] $T_K = 1/2(U\Gamma)^{1/2}\exp[\pi\epsilon(\epsilon+U)/\Gamma U]$. Since the weight of the equilibrium spectral density at the Fermi level is proportional to the linear conductance, an enhancement of the latter due to Kondo-assisted tunneling was predicted.[17,18] Typical values for quantum dots are $U \sim 1$ meV and $\Gamma \sim 50$ $\mu$eV, which, for $\epsilon \sim -\Gamma$, yield a Kondo temperature of the order $T_K \sim 50$ mK. Due to heating effects such temperatures are still hard to realize in realistic dots. A more pronounced feature was found for the nonlinear conductance, which shows a zero-bias maximum even for temperatures above the Kondo temperature.[13,14] At zero magnetic field the spectral density of each spin channel exhibits a Kondo resonance at each of the chemical potentials. An applied magnetic field causes the Kondo peaks to shift from the chemical potential by the Zeeman energy, in opposite directions for the different spin channels. As a consequence, Kondo-assisted tunneling can occur only if the bias voltage exceeds the Zeeman energy. Therefore, the zero-bias anomaly is split by an applied magnetic field.[14] These features have been observed experimentally by Ralph and Buhrman.[24] They measured the differential conductance through single-charge traps in a metallic quantum point contact. Although this system does not allow a controlled variation of the level position, the appearance of a zero-bias maximum with a peak height varying logarithmically with temperature clearly demonstrates the mechanism of Kondo-assisted tunneling. However, the detailed comparison of the line shape in the experiment and the existing theory showed significant deviations.

In this paper, we will describe an approach to calculate nonequilibrium properties of strongly correlated mesoscopic systems coupled to fermionic or bosonic baths via particle and energy exchange. It consists of a real-time diagrammatic approach closely related to path-integral methods formulated in connection with dissipation[27–29] or tunneling in metallic

 

junctions.[30–32] One of the difficulties of the present problem lies in the fact that we have to account for the Coulomb interaction in a nonperturbative way. Therefore, the standard many-body diagrammatic approaches are not sufficient (since Wick's theorem cannot be applied naively). We circumvent the problem by keeping track explicitly of the time evolution of the density matrix of the dot and tracing out only the bath degrees of freedom, which are assumed to be in equilibrium. The final diagrammatic language is set up by an expansion in the coupling to the fermionic reservoirs, whereas the strong correlations on the local system are exactly taken into account. The basic step is the calculation of transition and current rates between different states of the dot. We present an exact expression for these rates as the sum over all irreducible diagrams. The transition rate is used to set up a formally exact master equation from which the time-dependent probability distribution for the dot can be calculated. The current rate is generally not identical to the transition rate since it contains also the number of particles transferred to the reservoir where the current is calculated. This number can take arbitrary values if one considers all higher-order processes. The occupation probabilities multiplied with the current rates are used to calculate the current flowing through the system. In earlier publications, we have presented this technique in connection with tunneling through a metallic island with a continuum of states[33] and demonstrated the equivalence to path-integral methods.[34] There we used an approximation for the rate to sum up ''inelastic resonant tunneling'' processes to arbitrary order where different electrons tunnel coherently back and forth between the island and the reservoirs. Here we apply an equivalent approximation to describe resonant tunneling between metallic leads through an ultrasmall quantum dot with a single level. An important advantage of our approach is that we can solve the noninteracting limit exactly and can control systematically if this limit is contained within a given approximation for the correlated case. The theory is current conserving and can be used for the calculation of correlation functions or Green's functions as well.

For the case where the dot level is $M$-fold degenerate we recover for $M \geqslant 2$ and a low-lying dot level a Kondo peak in the spectral function. An applied transport voltage leads to a splitting of the Kondo peak (at $\mu_\alpha$, where $\alpha$ denotes the lead), which results in a zero-bias anomaly in the differential conductance such that the conductance has a maximum at $V=0$. On the other hand, if the dot level lies above the Fermi levels of the leads $\mu_\alpha$ we predict[15] a zero-bias anomaly in the conductance that has a minimum at $V=0$.

Several extensions will be considered. We study the case where the (spin) degeneracy of the dot level is lifted, e.g., by an applied magnetic field. In this case the Kondo peaks of both spin channels move apart from each other by the level spacing $\epsilon_\sigma - \epsilon_{\bar{\sigma}}$ and Kondo-assisted tunneling sets in only at transport voltages $eV$ exceeding this splitting. The calculated conductance agrees well with the experimental results of Ref. 24.

Furthermore, we account for inelastic interactions with bosonic modes coupled to the dot. They describe applied time-dependent fields, interaction with phonons, or the fluctuations in the electrodynamic environment. The investigation of this field has started only recently in connection with transport through interacting quantum dots. The classical regime ($\Gamma \gg T$) has been analyzed for time-dependent fields[11] and bosonic environments.[35] Photon- and boson-assisted tunneling lead here to resonant side peaks in the Coulomb oscillations that can be used to analyze the complete excitation spectrum of the dot. The results agree well with experiments.[36] In the Kondo regime it has been found[22] that time-dependent perturbations split the Kondo resonances, which leads to satellite anomalies in the differential conductance and offers the possibility to realize pump effects that are based purely on the presence of Kondo resonances. The linear ac conductance has been analyzed in Ref. 37. In this paper, we will investigate the influence of an external bosonic field on transport phenomena through ultrasmall quantum dots at low temperatures and small boson frequencies (compared to $\Gamma$). The emission and absorption of bosons causes additional Kondo singularities, for a one-mode field at $\mu_\alpha + n\omega_B$, where $n = \pm 1, \pm 2, \ldots$. Again, these resonances lead to corresponding anomalies in the differential conductance, which are inverted if the level position of the dot is moved through the Fermi energy.

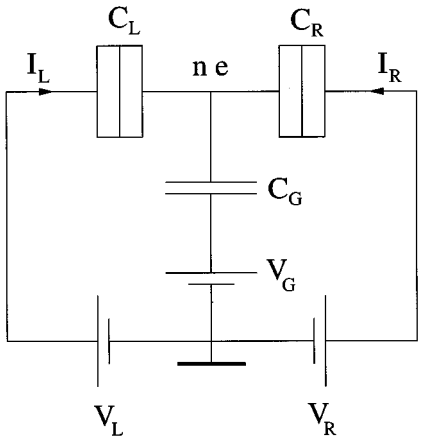


FIG. 1. Single-electron resistor.

## II. HAMILTONIAN

We concentrate here on a dot containing only one energy level $\epsilon_\sigma^{(0)}$ with degeneracy $M$. In a magnetic field, due to the Zeeman energy the level position is spin dependent. The dot is connected via high tunneling barriers to two large noninteracting reservoirs and coupled capacitively to an external gate voltage. The model Hamiltonian of this ''single-electron transistor'' (see Fig. 1) is

$$H = H_0 + H_T = H_D + \sum_{\alpha = L,R} H_\alpha + H_T . \tag{1}$$

Here $H_D$ is the Hamiltonian for the dot. It includes the Coulomb interaction of the dot electrons, which is described within the capacitance model of a single-electron transistor by the capacitances $C_L$ and $C_R$ for the left and right tunnel junctions and $C_G$ for the gate. Furthermore, the dot electrons are coupled to bosonic modes $\omega_q$ with electron-boson coupling $g_q$. Thus $H_D$ reads

$$H_D=\sum_\sigma \epsilon_\sigma^{(0)} n_\sigma + E_C(\hat{N}-n_G)^2 + \sum_q \omega_q d_q^\dagger d_q + \hat{N}\sum_q g_q(d_q+d_q^\dagger). \quad (2)$$

(Throughout this work, we set $\hbar=k=1$ and use the convention $e>0$.) The particle number on the dot with spin $\sigma$ is $n_\sigma=c_\sigma^\dagger c_\sigma$ and $\hat{N}=\Sigma_\sigma n_\sigma$. The scale of the charging energy is provided by $E_C\equiv e^2/2C$, where $C=C_L+C_R+C_G$ is the total capacitance of the system. The transistor can be tuned by the gate voltage $V_G$ via $en_G=C_LV_L+C_RV_R+C_GV_G$. We remark here that $H$ is invariant under a global shift of all energies. Therefore, we can always choose symmetric bias, $V_L=-V_R=V/2$.

The next term in Eq. (1), $H_\alpha=\Sigma_{k\sigma}\epsilon_{k\alpha}a_{k\sigma\alpha}^\dagger a_{k\sigma\alpha}$, describes the reservoir $\alpha$ of noninteracting electrons in the leads. Finally, the dot is coupled via tunnel barriers to the left and right lead. This coupling is described by the tunnel Hamiltonian

$$H_T=\sum_{k,\sigma,\alpha}(T_k^\alpha a_{k\sigma\alpha}^\dagger c_\sigma+\text{H.c.}). \quad (3)$$

The bosonic modes can represent interaction with phonons[38–40] or fluctuations of the electrodynamic environment[41–44] very similar to the Caldeira-Leggett model.[45] For our theory no assumption is needed for the specific kind of the modes $\omega_q$ and the couplings $g_q$. In this way we are able to present a general result for the current that shows the influence of inelastic interactions for an arbitrary environment.

The capacitive model is equivalent to the Anderson Hamiltonian, which we obtain by defining the interaction $U_0=2E_C$ and shifting the level position $\epsilon_\sigma^{(0)}+2E_C-eV_GC_G/C-a_ceV/2\to\epsilon_\sigma^{(0)}(V,V_G)$. The asymmetry factor $a_c=(C_L-C_R)/C$ accounts for a different capacitive coupling of the left and right leads. We see here that the effective level position in the Anderson model depends on the gate voltage as well as, due to $a_c$, on the transport voltage. The dot is then described by

$$H_D=\sum_\sigma \epsilon_\sigma^{(0)}(V,V_G)n_\sigma + U_0\sum_{\sigma<\sigma'} n_\sigma n_{\sigma'} + \sum_q \omega_q d_q^\dagger d_q + \hat{N}\sum_q g_q(d_q+d_q^\dagger). \quad (4)$$

A unitary transformation[46] with $V=\exp(-i\hat{N}\varphi)$ and $\varphi=i\Sigma_q(g_q/\omega_q)(d_q^\dagger-d_q)$ yields $H=VHV^{-1}=H_0+H_T$, where $H_0=H_R+H_D$,

$$\overline{H_D}=\sum_\sigma \epsilon_\sigma n_\sigma + U\sum_{\sigma<\sigma'} n_\sigma n_{\sigma'} + \sum_q \omega_q d_q^\dagger d_q, \quad (5)$$

and

$$\overline{H_T}=\sum_{k,\sigma,\alpha}(T_k^\alpha a_{k\sigma\alpha}^\dagger c_\sigma e^{i\varphi}+\text{H.c.}). \quad (6)$$

The electron-boson interaction renormalizes the level position and the Coulomb repulsion $\epsilon_\sigma=\epsilon_\sigma^{(0)}-\Sigma_q g_q^2/\omega_q$ and $U=U_0-2\Sigma_q g_q^2/\omega_q$ and the tunneling term acquires phase factors $e^{\pm i\varphi}$.

For strong Coulomb repulsion $U$ we restrict ourselves to states with $N=0,1$. In lowest-order perturbation theory the rates for tunneling into and out of the dot to reservoir $\alpha$ are

$$2\pi\gamma_\alpha^\pm(E)=2\pi\int dE'\,\overline{\gamma_\alpha^\mp}(E')P^\pm(E-E'), \quad (7)$$

where $2\pi\overline{\gamma_\alpha^\mp}(E)=\Gamma_\alpha(E)f_\alpha^\mp(E)$ is the classical rate without bosons, $\Gamma_\alpha(E)=2\pi\Sigma_k|T_k^\alpha|^2\delta(E-\epsilon_{k\alpha})$, and $f_\alpha^+(E)$ is the Fermi distribution of reservoir $\alpha$ with electrochemical potential $\mu_\alpha$, while $f_\alpha^-(E)=1-f_\alpha^+(E)$. Finally,

$$P^\pm(E)=\frac{1}{2\pi}\int dt e^{iEt}\langle e^{i\varphi(0)}e^{-i\varphi(\pm t)}\rangle_0 \quad (8)$$

describes the probability that an electron absorbs ($P^+$) or emits ($P^-$) the boson energy $E$.[41–43] The expectation value is taken with the free boson Hamiltonian. These probabilities satisfy the condition of detailed balance[47]

$$P^-(E)=P^+(-E)=e^{\beta E}P^+(E). \quad (9)$$

The classical rates combined with a master equation are sufficient in the perturbative regime $\Gamma=\Sigma_\alpha\Gamma_\alpha\ll T$.[35]

In order to go beyond the perturbative regime, we need a nonperturbative treatment of the tunneling, where quantum fluctuations yield finite lifetime broadening and renormalization effects of the dot levels. As an illustration we first assume that (for $B=0$) the broadening is given by the sum of the classical transition rates Eq. (7). Using the Kramers-Kronig relation we deduce the renormalization and obtain for the self-energy

$$\sigma(E)=\int dE'\,\frac{M\gamma^+(E')+\gamma^-(E')}{E-E'+i0^+}. \quad (10)$$

where $\gamma^\pm=\Sigma_\alpha\gamma_\alpha^\pm$. The aim of the present paper is to test and extend this simple physical picture within a systematic and conserving theory for all Green's functions and the current. To achieve this we use a real-time technique developed in Refs. 34, 33, and 15 that provides a natural generalization of the classical and cotunneling theory to the physics of resonant tunneling.

## III. DIAGRAMMATIC TECHNIQUE

A quantum-statistical expectation value of an operator $A$ at time $t$ is given by

$$\langle A(t)\rangle=\text{tr}[\rho_0 A(t)_{\overline{H}}], \quad (11)$$

where $A(t)_{\overline{H}}=\exp[i\overline{H}(t-t_0)]A\exp[-i\overline{H}(t-t_0)]$ is the operator in Heisenberg picture with respect to the initial time $t_0$. Permutation under the trace yields $\langle A(t)\rangle=\text{tr}[\rho(t)A]$, with $A$ in Schrödinger picture. The density matrix $\rho(t)$ evolves in time via $\rho(t)=e^{-i\overline{H}(t-t_0)}\rho(t_0)e^{i\overline{H}(t-t_0)}$. We assume that the initial density matrix $\rho_0=\rho(t_0)$ factorizes into parts for the dot electrons, the bosons, and the leads:

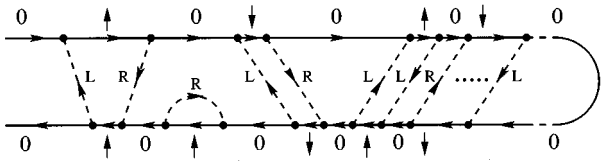


FIG. 2. Diagram showing various tunneling processes: sequential tunneling in the left and right junctions, a term preserving the norm, a cotunneling process, and resonant tunneling.

$$\rho_0=\rho_0^D\rho_0^B\prod_\alpha \rho_0^\alpha. \tag{12}$$

The leads are treated as large equilibrium reservoirs with fixed electrochemical potentials $\mu_\alpha=-eV_\alpha$. Therefore, we describe the electrons in the leads by Fermi functions $f_\alpha(E)$ and the density matrix reads

$$\rho_0^\alpha=\frac{1}{Z_0^\alpha}\exp[-\beta(H_\alpha-\mu_\alpha N_\alpha)], \tag{13}$$

where $\beta=1/T$ and $N_\alpha=\Sigma_{k,\sigma}a_{k\sigma\alpha}^\dagger a_{k\sigma\alpha}$ the number of electrons in the lead $\alpha$. The normalization factor $Z_0^\alpha$ is determined by $\mathrm{tr}\rho_0^\alpha=1$. The boson part reads

$$\rho_0^B=\frac{1}{Z_0^B}\exp\left[-\beta_B\sum_q \omega_q d_q^\dagger d_q\right]. \tag{14}$$

The temperature of the boson bath $T_B=1/\beta_B$ may differ in real experiments from the electron temperature $T$.

For the initial distribution of the dot we assume that it is diagonal in the many-body *dot* states $|\chi\rangle$, which include the strong correlations within the quantum dot but are assumed to have fixed occupation numbers

$$\rho_0^D=\sum_\chi P_\chi^0|\chi\rangle\langle\chi|, \tag{15}$$

with $\Sigma_\chi P_\chi^0=1$. We will see later that in the stationary limit, i.e., when $t_0$ is shifted to $-\infty$ all the physical quantities are independent of the choice of $P_\chi^0$.

In the following, it is convenient to change to the interaction picture with respect to $\overline{H_0}$. This implies $A(t)_{\overline{H}}=\widetilde{T}\exp[-i\int_t^{t_0}dt'\overline{H_T}(t')_I]A(t)_I T\exp[-i\int_{t_0}^t dt'\overline{H_T}(t')_I]$ in which $T$ is the time-ordering operator and $\widetilde{T}$ denotes the anti-time-ordering operator. We write the integrals as one contour integral $\int_K dt'\cdots$ over the *Keldysh contour*. It is parametrized by the ''time'' $t'$, which first runs forward from $t_0$ to $t$ and then backward from $t$ to $t_0$. In diagrammatic language, the Keldysh contour is represented by horizontal lines running from the left to the right and then back to the left (see Fig. 2). We find

$$\langle A(t)\rangle=\mathrm{tr}\left[\rho_0 T_K\exp\left(-i\int_K dt'\overline{H_T}(t')_I\right)A(t)_I\right]. \tag{16}$$

Here we have introduced the Keldysh time-ordering operator $T_K$, which orders all following operators along the Keldysh contour such that the one with the later time along the Keldysh contour appears at a more left position (without any sign change for an exchange of Fermi operators).

In the following we will encounter also higher-order correlation functions of the type $\langle T_K A_1(t_1)_I A_2(t_2)_I\cdots A_n(t_n)_I\rangle$. The final time $t$ of the Keldysh contour is then given by $\max\{t_1,\ldots,t_n\}$.

For a diagrammatic description we expand the exponential with respect to the tunneling Hamiltonian and obtain

$$\left\langle T_K\prod_{i=1}^n A_i(t_i)\right\rangle=\mathrm{tr}\Bigg[\rho_0\sum_{m=0}^\infty(-i)^m\int_K dt_1'\int_K dt_2'\cdots\int_K dt_m' \times T_K\Bigg\{\overline{H_T}(t_1')_I\overline{H_T}(t_2')_I\cdots\overline{H_T}(t_m')_I \times\prod_{i=1}^n A_i(t_i)_I\Bigg\}\Bigg],\quad t_1'>t_2'>\cdots>t_m', \tag{17}$$

in which the relation $t_1'>t_2'>\cdots>t_m'$ has to be understood with respect to the Keldysh contour. The time-ordering operator $T_K$ acts also in the operators $A_i(t_i)_I$ and puts them in the right place between the tunneling Hamiltonians.

The next task is to perform the trace of each term of the expansion. We insert the tunnel Hamiltonian (6) and notice that the Hamiltonian $\overline{H_0}$ is bilinear in the lead electron operators. For this reason, Wick's theorem holds for these degrees of freedom, i.e., the lead electron operators are contracted in pairs. This includes contractions between pairs of field operators from $H_T$ as well as contractions to lead electron operators that can be present in the operators $A_i$. These contractions are given by equilibrium distribution functions. For the dot electrons, the situation is different. The Coulomb interaction is expressed by a quartic term of dot electron operators. Therefore, Wick's theorem does not hold for this part of the system. A product of dot electron operators cannot be contracted into pairs, but has to be treated explicitly. The trace over the bosonic part, however, poses no problem. Each tunneling term contains an exponential $e^{\pm i\varphi}$ of the bosonic operators $\varphi$. The trace over the product of such exponentials can be performed easily [see Eq. (20)] provided that the operator $A$ also contains only such exponentials.

### A. Rules

With regard to the applications discussed in Secs. III B and III C, we assume here that the operators $A_i$ (representing ''external vertices'') depend on the lead and boson degrees of freedom only in the form

$$A_i=A_i\Bigg(\sum_k T_k^\alpha a_{k\sigma\alpha}^\dagger c_\sigma e^{i\varphi},\ \sum_k T_k^{\alpha *}c_\sigma^\dagger a_{k\sigma\alpha}e^{-i\varphi}, c_\sigma e^{i\varphi}, c_\sigma^\dagger e^{-i\varphi}\Bigg). \tag{18}$$

Each term of the expansion Eq. (17) is visualized by a diagram (see Fig. 2). There is a forward and a backward propagator symbolized by the upper and the lower horizontal line, running from $t_0$ to $t$ and back from $t$ to $t_0$, respectively. Along this time path, we arrange internal and external verti-

ces according to their time ordering. The internal vertices emerge from the insertion of the tunneling Hamiltonian (6) into the expansion (17). Each of them corresponds to a product of a lead and a dot electron operator and a phase factor $e^{\pm i\varphi}$. After integrating out the lead degrees of freedom, all vertices (either internal or external) containing a lead electron operator are connected in pairs by directed tunneling lines (dashed lines) $\overline{\gamma_\alpha^K}(t,t')$ from $t'$ to $t$, with $\overline{\gamma_\alpha^K}(t,t')=\overline{\gamma_\alpha^+}(t-t')$ for $t<t'$ and $\overline{\gamma_\alpha^K}(t,t')=\overline{\gamma_\alpha^-}(t-t')$ for $t>t'$ with respect to the Keldysh contour with $\overline{\gamma_\alpha^\pm}(t)=\int dE e^{-iEt}\overline{\gamma_\alpha^\pm}(E)$. These tunneling lines represent contractions of lead electron operators.

There are vertices from which a tunneling line leaves [representing $a_{k\sigma\alpha}^\dagger(t)c_\sigma(t)e^{i\varphi(t)}$, which removes a dot electron with spin $\sigma$] and others to which a tunneling line enters [representing $c_\sigma^\dagger(t)a_{k\sigma\alpha}(t)e^{-i\varphi(t)}$, which adds a dot electron with spin $\sigma$]. Fermi statistics, furthermore, yield a minus sign for each crossing of tunneling lines.

In the interaction picture the dot electron operators get exponential factors that contain the energies $\epsilon_\chi$ of the many-body dot states $\chi$ given by $\epsilon_\chi|\chi\rangle=H_D|\chi\rangle$. The order of the electron operators may induce, furthermore, a minus sign due to Fermi statistics.

The trace over the boson operators gives rise to a factor of the form

$$C_B(t_1,t_2,\ldots,t_m,t_1',t_2',\ldots,t_{m'}')=\langle T_K[e^{-i\varphi(t_1)}e^{-i\varphi(t_2)}\cdots e^{-i\varphi(t_m)}e^{i\varphi(t_1')}e^{i\varphi(t_2')}\cdots e^{i\varphi(t_{m'}')}]\rangle. \tag{19}$$

Since $\varphi$ is linear in the boson operators, we get

$$C_B(t_1,t_2,\ldots,t_m,t_1',t_2',\ldots,t_{m'}')=\prod_{i<j}P^K(t_i,t_j)^{-1}\prod_{i<j}P^K(t_i',t_j')^{-1}\prod_{i,j}P^K(t_i,t_j'). \tag{20}$$

We write $P^K(t,t')=P^+(t,t')$ for $t<t'$ and $P^K(t,t')=P^-(t,t')$ for $t>t'$ on the Keldysh contour with $P^\pm(t)=\int dE e^{-iEt}P^\pm(E)$. In diagrammatic language, we represent the factors $P^K$ by boson lines connecting each vertex with each other. A summary of these rules are given in Appendix A.

In order to calculate stationary transport properties it is convenient to change to an energy representation. Without loss of generality we assume that the times $t_1,\ldots,t_n$ of the correlation function (17) are ordered on the real axis according to $t_n<t_{n-1}<\cdots<t_1=t$. This may be different from the ordering on the Keldysh contour, which depends on whether the times lie on the upper or lower branch. In the stationary limit we can set $t_0=-\infty$ and $t=t_1=0$.

We consider the Laplace transform

$$G(E_2,E_3,\ldots,E_n)=(-i)^{n-1}\int_{-\infty}^0 dt_2\int_{-\infty}^{t_2}dt_3\cdots\int_{-\infty}^{t_{n-1}}dt_n e^{iE_2t_2}\times e^{iE_3t_3}\cdots e^{iE_nt_n}\langle T_K A_1(0)A_2(t_2)\cdots A_n(t_n)\rangle. \tag{21}$$

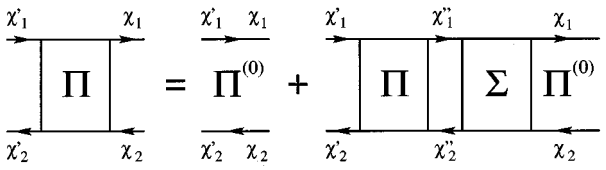


FIG. 3. Iteration of processes for the propagator $\Pi$.

We will account for the exponential factors $\exp(iE_it_i)$ $(i=2,\ldots,n)$ by drawing directed virtual lines from the external vertices with time $t_i$ to the last vertex with time $t_1=0$ and assigning the energy $E_i$ to this virtual line.

Performing the time integrals, we end up with diagrammatic rules in an energy representation. These rules are summarized in Appendix B.

### B. Master equation and stationary probabilities

In this section we will derive a formally exact expression for the central object of this paper: the quantum-mechanical transition rate $\Sigma_{\chi',\chi}(t',t)$ for the reduced system (the dot) to go from a state $\chi'$ at time $t'$ to a state $\chi$ at time $t$. This rate will serve as input for a formally exact and time-dependent master equation, which, in principle, could be used to calculate all occupation probabilities of the dot as a function of time for an arbitrary initial state. Similar master equations are well known and successfully applied in connection with macroscopic quantum coherence phenomena in spin boson models.[28,29,48] The connection to these path-integral approaches will be described in Ref. 57.

A matrix element of the reduced density matrix of the dot at time $t$, $P_{\chi_2}^{\chi_1}(t)$, is given by the quantum-statistical expectation value of the projector $(|\chi_2\rangle\langle\chi_1|)(t)$,

$$P_{\chi_2}^{\chi_1}(t)=\langle(|\chi_2\rangle\langle\chi_1|)(t)\rangle, \tag{22}$$

i.e., we have to set $n=1$ and $A_1=|\chi_2\rangle\langle\chi_1|$ in Eq. (17). The reduced density matrix commutes with the particle number on the dot. Thus the operator $|\chi_2\rangle\langle\chi_1|$ is unaffected by the unitary transformation and no tunneling and boson line emerges from this external vertex. The matrix element $P_{\chi_2}^{\chi_1}(t)$ can be expressed by the reduced propagator $\Pi_{\chi_2',\chi_2}^{\chi_1',\chi_1}(t',t)$ from $\chi_1'$ at time $t'$ forward to $\chi_1$ at time $t$ and then from $\chi_2$ at time $t$ backward to $\chi_2'$ at time $t'$,

$$P_{\chi_2}^{\chi_1}(t)=\sum_{\chi_1',\chi_2'}P_{\chi_2'}^{\chi_1'}(t')\Pi_{\chi_2',\chi_2}^{\chi_1',\chi_1}(t',t). \tag{23}$$

The propagator is the sum of all diagrams with the given states at the ends and can be expressed by an irreducible self-energy part $\Sigma_{\chi_2',\chi_2}^{\chi_1',\chi_1}(t',t)$, defined as the sum of all diagrams in which any vertical line cutting through them crosses at least one tunneling or boson line. The propagators for the four lines attached to the self-energy are not included in $\Sigma_{\chi_2',\chi_2}^{\chi_1',\chi_1}(t',t)$. We obtain an iteration in the style of a Dyson equation (see Fig. 3),

$$\Pi^{\chi_1',\chi_1}_{\chi_2',\chi_2}(t',t)=\Pi^{(0)\chi_1}_{\chi_2}(t',t)\,\delta_{\chi_1,\chi_1'}\delta_{\chi_2,\chi_2'} + \sum_{\chi_1'',\chi_2''}\int_{t'}^{t}dt_2\int_{t'}^{t_2}dt_1\Pi^{\chi_1',\chi_1''}_{\chi_2',\chi_2''}(t',t_1) \times\Sigma^{\chi_1'',\chi_1}_{\chi_2'',\chi_2}(t_1,t_2)\Pi^{(0)\chi_1}_{\chi_2}(t_2,t), \tag{24}$$

where $\Pi^{(0)\chi_1}_{\chi_2}(t',t)=\exp[-i(\epsilon_{\chi_1}-\epsilon_{\chi_2})(t-t')]$ is the propagator of the isolated quantum dot. Multiplying this equation with $P^{\chi_1'}_{\chi_2'}(t')$, summing over the states $\chi_1',\chi_2'$, and differentiating with respect to $t$, we obtain, together with Eq. (23) and setting $t'=t_0$,

$$\frac{d}{dt}P^{\chi_1}_{\chi_2}(t)+i(\epsilon_{\chi_1}-\epsilon_{\chi_2})P^{\chi_1}_{\chi_2}(t) = \sum_{\chi_1',\chi_2'}\int_{t_0}^{t}dt'\,P^{\chi_1'}_{\chi_2'}(t')\Sigma^{\chi_1',\chi_1}_{\chi_2',\chi_2}(t',t). \tag{25}$$

This formally exact equation is the most general kinetic equation for the reduced density matrix of the dot. No assumption is necessary for the initial state and the integral kernel $\Sigma$ on the right-hand side shows that memory effects are fully taken into account.

The equation simplifies considerably if we assume that the initial density matrix is diagonal. In the general case, this does not imply that the reduced density matrix stays diagonal for all times. However, for the special case of the Anderson model considered here, spin conservation implies that the reduced density matrix will be diagonal for all times $t>t_0$. Hence we consider $\Sigma_{\chi',\chi}\equiv\Sigma^{\chi',\chi}_{\chi',\chi}$ and obtain, from (25),

$$\frac{d}{dt}P_\chi(t)=\sum_{\chi'}\int_{t_0}^{t}dt'\,P_{\chi'}(t')\Sigma_{\chi',\chi}(t',t), \tag{26}$$

where $P_\chi(t)\equiv P^\chi_\chi(t)$ denotes the probability to be in state $\chi$ at time $t$. For a time-translational invariant system, the time-dependent rates $\Sigma_{\chi',\chi}(t',t)$ depend only on the time difference $\Sigma_{\chi',\chi}(t'-t)$. Performing the Laplace transform of Eq. (26), one can then study the time evolution of arbitrary initial probability distributions into the stationary state.

By attaching the rightmost vertex of each diagram $\Sigma$ to the upper and lower propagators, the minus sign for each vertex on the backward propagator yields $\Sigma_\chi\Sigma_{\chi',\chi}(t',t)=0$, which allows us to rewrite Eq. (26) in the form

$$\frac{d}{dt}P_\chi(t)=\sum_{\chi'\neq\chi}\int_{t_0}^{t}dt'[P_{\chi'}(t')\Sigma_{\chi',\chi}(t',t) - P_\chi(t')\Sigma_{\chi,\chi'}(t',t)]. \tag{27}$$

We obtain the structure of a master equation with transition rates given by $\Sigma_{\chi',\chi}(t',t)$.

The stationary distribution is given by

$$P^{\rm st}_\chi=\lim_{t\to\infty}P_\chi(t)=\lim_{t_0\to-\infty}P_\chi(0) \tag{28}$$


FIG. 4. Graphical representation of the current $I_\alpha$ through lead $\alpha$. Internal vertices are not indicated.

and is *not* the equilibrium one if the electrochemical potentials of the leads are different. From (26) and (27) we obtain

$$0=\sum_{\chi'}P^{\rm st}_{\chi'}\Sigma_{\chi',\chi}=\sum_{\chi'\neq\chi}[P^{\rm st}_{\chi'}\Sigma_{\chi',\chi}-P^{\rm st}_\chi\Sigma_{\chi,\chi'}], \tag{29}$$

where

$$\Sigma_{\chi',\chi}=i\int_{-\infty}^{0}dt'\Sigma_{\chi',\chi}(t',0) \tag{30}$$

can be calculated directly by using our diagrammatic rules in energy space. The prefactor $i$ in (30) together with the $m-1$ time integrations over the internal vertices in $\Sigma$ gives a factor $i^m$ in (B1) that cancels the factor $(-i)^m$ from rule 5.

The self-energy part $\Sigma_{\chi',\chi}$ is purely imaginary. This can be seen by changing the vertical positions of all vertices on the Keldysh contour (without changing their horizontal position) and reversing the direction of all tunneling and boson lines. Consequently, only the energy differences $\Delta E_j$ from rule $2'$ will change sign. Since the number of vertices is even (all tunneling vertices are coupled in pairs by tunneling lines), there is no sign change due to rule $5'$ and the number of resolvents is odd. Thus the whole diagram has been changed to its conjugate complex up to a sign.

### C. Tunneling current

The tunneling current flowing into reservoir $\alpha$ is defined by $I_\alpha(t)=e(d/dt)\langle N_\alpha(t)\rangle=ie\langle[H,N_\alpha](t)\rangle$, which is equivalent to

$$I_\alpha(t)=-ie\sum_{k,\sigma}\{T^\alpha_k\langle(a^\dagger_{k\sigma\alpha}c_\sigma e^{i\varphi})(t)\rangle - T^{\alpha *}_k\langle(c^\dagger_\sigma a_{k\sigma\alpha}e^{-i\varphi})(t)\rangle\}. \tag{31}$$

The tunneling current is an expectation value of a product of a dot, boson, and reservoir electron operator (see Fig. 4). We obtain

$$I_\alpha(t)=e\sum_{\chi,\chi'}\int_{t_0}^{t}dt'\,P_{\chi'}(t')\Sigma^{\alpha+}_{\chi',\chi}(t',t) =-e\sum_{\chi,\chi'}\int_{t_0}^{t}dt'\,P_{\chi'}(t')\Sigma^{\alpha-}_{\chi',\chi}(t',t), \tag{32}$$

where the partial self-energies $\Sigma^{\alpha\pm}_{\chi',\chi}(t',t)$ are parts of the total self-energy

$$\Sigma_{\chi',\chi}(t',t)=\sum_\alpha\{\Sigma^{\alpha+}_{\chi',\chi}(t',t)+\Sigma^{\alpha-}_{\chi',\chi}(t',t)\}. \tag{33}$$

They describe processes in which the rightmost tunneling line corresponds to reservoir $\alpha$ and is an outgoing (incoming) line if the rightmost vertex lies on the upper propagator

or an incoming (outgoing) line if the rightmost vertex lies on the lower propagator. Their physical meaning is displayed by the current formula (32), which shows that they give the total contribution to the current rate. We can relate them to an intuitively more physical object, namely, the rate $\Sigma^{\alpha p}_{\chi',\chi}(t',t)$, $p=0,\pm1,\pm2,\ldots$, which describes the transition rate where $p$ particles are transferred to reservoir $\alpha$. Within our graphical language $\Sigma^{\alpha p}_{\chi',\chi}(t',t)$ is given by all diagrams where the number of tunneling lines with reservoir index $\alpha$ running from the forward to the backward propagator minus the number of tunneling lines with reservoir index $\alpha$ running from the backward to the forward propagator is given by $p$. We obtain

$$\sum_{\chi} \Sigma^{\alpha\pm}_{\chi',\chi}(t',t)=\pm\sum_{\chi}\sum_{p} p\Sigma^{\alpha p}_{\chi',\chi}(t',t). \tag{34}$$

This relation together with current conservation is proven in Appendix C. The factor $p$ shows clearly that $\Sigma^{\alpha\pm}$ describes the contribution to the current rate. In contrast to lowest-order processes, i.e., the golden rule rate, where $p$ can only take the values $\pm1$, $p$ can be arbitrary for higher-order processes. Nevertheless, Eq. (33) shows that the current rate can be calculated as a partial selection of diagrams already contained in the total transition rate $\Sigma_{\chi',\chi}$.

We emphasize that the current formula (32) together with the master equation (26) constitutes a complete theory to describe time-dependent phenomena starting from an arbitrary diagonal initial state. The original problem has now been shifted to the evaluation of the various self-energy diagrams that correspond to transition and current rates. The self-energies are defined by a set of irreducible diagrams and thus their corresponding perturbation expansion in the number of tunneling lines is a well-defined series and contains no divergent time integrals.

For time-translational invariant systems the current rates $\Sigma^{\alpha\pm}_{\chi',\chi}(t',t)$ depend only on the time difference $t'-t$. To calculate the stationary current we define in analogy to (30)

$$\Sigma^{\alpha\pm}_{\chi',\chi}=i\int_{-\infty}^{0}dt'\Sigma^{\alpha\pm}_{\chi',\chi}(t',0), \tag{35}$$

which again can be calculated directly with our diagrammatic rules in energy space. The stationary current is then given by

$$I^{\rm st}_{\alpha}=-ie\sum_{\chi,\chi'} P^{\rm st}_{\chi'}\Sigma^{\alpha+}_{\chi',\chi}=ie\sum_{\chi,\chi'} P^{\rm st}_{\chi'}\Sigma^{\alpha-}_{\chi',\chi}. \tag{36}$$

### D. Green's functions

After the unitary transformation the Green's functions of the dot electrons read

$$G^{>}_{\sigma}(t,t')=-i\langle(c_\sigma e^{i\varphi})(t)(c^{\dagger}_{\sigma}e^{-i\varphi})(t')\rangle, \tag{37}$$

$$G^{<}_{\sigma}(t,t')=i\langle(c^{\dagger}_{\sigma}e^{-i\varphi})(t')(c_\sigma e^{i\varphi})(t)\rangle. \tag{38}$$

Here $G^{>}_{\sigma}$ and $G^{<}_{\sigma}$ are independent quantities since we do not assume equilibrium. For time-translational invariant systems, the Green's functions depend only on the time difference

$$I^{\rm st}_{\alpha}=2e\ \mathrm{Im}\sum_{\sigma}$$


FIG. 5. Graphical representation of the relation between the current and the correlation functions. Here the line connecting the external vertices is a real one. Internal vertices are not indicated.

$G(t,t')=G(t-t')$. The Fourier transform $G(E)=\int dt e^{iEt}G(t)$ can be written in the form

$$G^{>}_{\sigma}(E)=2i\ \mathrm{Im}(-i)\int_{-\infty}^{0}dt e^{-iEt}\times\langle T_K(c_\sigma e^{i\varphi})(0)(c^{\dagger}_{\sigma}e^{-i\varphi})(t^{+})\rangle, \tag{39}$$

$$G^{<}_{\sigma}(E)=-2i\ \mathrm{Im}(-i)\int_{-\infty}^{0}dt e^{-iEt}\times\langle T_K(c_\sigma e^{i\varphi})(0)(c^{\dagger}_{\sigma}e^{-i\varphi})(t^{-})\rangle, \tag{40}$$

where $t^{\pm}$ means that the time $t$ lies on the upper (lower) branch of the Keldysh contour. Note that the time ordering is defined here by a pure ordering along the Keldysh contour without any sign change if we interchange fermion operators. The integrals can be calculated like Eq. (21), whereby instead of assigning the energy $-E$ to the virtual line connecting the external vertices one can change the direction of the line and assign the energy $E$.

In order to relate the current to the Green's functions of the dot we consider the first diagram on the right-hand side of Fig. 4 (the second one is just the conjugate complex). The external vertex can be contracted by a tunneling line to either the upper or lower propagator and we recover immediately the structure of the Green's functions $G^{>}$ and $G^{<}$, respectively (see Fig. 5). We recover for the stationary current the relation[50,13,14]

$$I^{\rm st}_{\alpha}=-ie\sum_{\sigma}\int dE\{\gamma^{+}_{\alpha}(E)G^{>}_{\sigma}(E)+\gamma^{-}_{\alpha}(E)G^{<}_{\sigma}(E)\}. \tag{41}$$

In the case that the couplings to the leads have the same energy dependence $\Gamma_{\alpha}(E)/\Gamma_{\alpha'}(E)=\lambda_{\alpha,\alpha'}$, this can be written in the form (which was already derived in Ref. 14)

$$I^{\rm st}_{\alpha}=e\sum_{\alpha'}\sum_{\sigma}\int dE\frac{\Gamma_{\alpha}(E)\Gamma_{\alpha'}(E)}{\Sigma_{\alpha''}\Gamma_{\alpha''}(E)}\rho_{\sigma}(E)[f^{+}_{\alpha'}(E)-f^{+}_{\alpha}(E)]. \tag{42}$$

Here we used the relation between the Green's functions $G^{<}_{\sigma}, G^{>}_{\sigma}$ and spectral density $\rho_\sigma\equiv G^{<}_{\sigma}-G^{>}_{\sigma}/2\pi i$.

## IV. RESULTS

What we have done so far is to derive a diagrammatic language that allows a systematic description of transport processes. Furthermore, we have shown how the physical quantities of interest, the stationary probability distribution and the current, can be obtained if we know the value of special diagrams. In this section, we will now explicitly calculate the value of the corresponding diagrams.

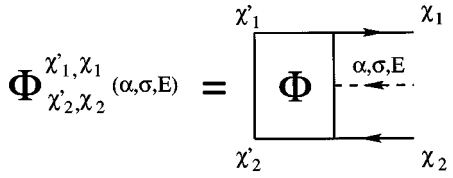


FIG. 6. Definition of $\phi$, which denotes a part of a diagram with an open tunneling line entering from the right.

We consider here the case of strong Coulomb repulsion $U$, i.e., we restrict ourselves to the states with $N=0,1$. Diagrams in which a higher occupancy occurs do not contribute since they have resolvents of the order $1/U$.

In the following, the index $\sigma$ labels the singly occupied state with spin $\sigma=1,\ldots,M$. The label $\chi$ additionally allows an empty dot, $\chi=0,1,\ldots,M$.

In general, we cannot sum up *all* possible diagrams. Therefore, we have to find a systematic criterion that diagrams should be retained and summed.

The simplest approximation is to neglect all diagrams where two or more tunneling lines overlap in time (see the leftmost diagram parts in Fig. 2). This means that we include those processes that are also described by the master equation with rates obtained in lowest-order perturbation theory (sequential tunneling), which is a good description at high temperature $\Gamma \ll T$.

In situations when sequential tunneling is suppressed by Coulomb blockade, the lowest-order contribution to the current arises due to cotunneling. The rates for a process in which an electron enters the dot from the left lead and leaves to right one is described by diagrams with two overlapping lines (see the diagram part in the middle of Fig. 2).

At lower temperature the perturbative approach is not sufficient. Higher-order processes become important. In a generalization to cotunneling we have to take into account irreducible diagrams with an arbitrary number of correlated tunneling processes, i.e., we include resonant tunneling.

Similar to the case of metallic islands,[33,34] we proceed in a conserving approximation, taking into account nondiagonal matrix elements of the total density matrix up to the difference of one electron-hole pair excitation in the leads. The graphical representation of this constriction is that only diagrams in which any vertical line will cut at most two tunneling lines are taken into account.

We give two arguments why this class of diagrams is the most important one. First, since we treat the leads as large equilibrium reservoirs there should be a tendency of the system to stay close to diagonal states. Second, our approximation contains the exact solution for the noninteracting limit $U=0$: if there is no electron-electron interaction in the dot, electrons with different spin do not influence each other, so that this limit is described within our model by choosing $M=1$. In this case, the selected diagrams are the only contributing ones. The sum of all other, more complicated, diagrams is zero.

Furthermore, we include only boson lines between vertices that are already connected by tunneling lines, i.e.,

$$C_B(t_1,t_2,\ldots,t_m,t_1',t_2',\ldots,t_m') \approx \prod_{i=1}^{m} P^K(t_i,t_i'), \quad (43)$$

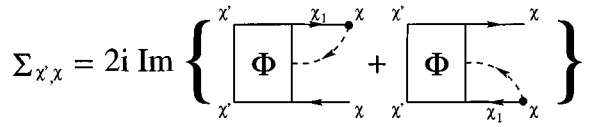


FIG. 7. Irreducible self-energy obtained by attaching the open tunneling line of $\phi$ and $\phi^*$ to the upper and lower propagators.

where the pairs $t_i,t_i'$ are already coupled by tunneling lines running from $t_i'$ to $t_i$. This amounts to a dressing of the tunneling lines $\overline{\gamma \to \gamma}$. This approximation, while neglecting many diagrams, describes well the spectral density of the dot at resonance points. The reason is that position and value of the peaks of the spectral density are determined by a self-energy $\sigma$ [see Eq. (49)], which is calculated here in lowest-order perturbation theory in $\Gamma$ including the bosons. Higher orders are small for high tunnel barriers.

First, we relate the rate $\Sigma_{\chi',\chi}$ to an irreducible diagram labeled by $\phi^{\chi_1',\chi_1}_{\chi_2',\chi_2}(\alpha,\sigma,E)$ (see Fig. 6). It has an open tunneling line associated with tunneling of an electron with spin $\sigma$ in the junction $\alpha$ carrying the energy $E$. The line is directed from the right to the left and its value together with the corresponding resolvent is included in $\phi$. The self-energy is then constructed by attaching the open tunneling line of these diagrams to the upper and lower propagators (see Fig. 7) with the result

$$\begin{aligned}\Sigma_{\chi',\chi} &= 2i\ \mathrm{Im} \int dE \sum_{\sigma,\alpha} \sum_{\chi_1} \{\langle\chi|c_\sigma|\chi_1\rangle \phi^{\chi',\chi_1}_{\chi',\chi}(\alpha,\sigma,E) \\ &\quad - \langle\chi_1|c_\sigma|\chi\rangle \phi^{\chi',\chi}_{\chi',\chi_1}(\alpha,\sigma,E)\} \\ &= \sum_\alpha \{\Sigma^{\alpha+}_{\chi',\chi} + \Sigma^{\alpha-}_{\chi',\chi}\}, \end{aligned} \quad (44)$$

where the current rates $\Sigma^{\alpha\pm}_{\chi',\chi}$ correspond to the first and second terms, respectively. Again we have made use of the fact that a diagram becomes the conjugate complex if we change the vertical position of all vertices and the direction of all

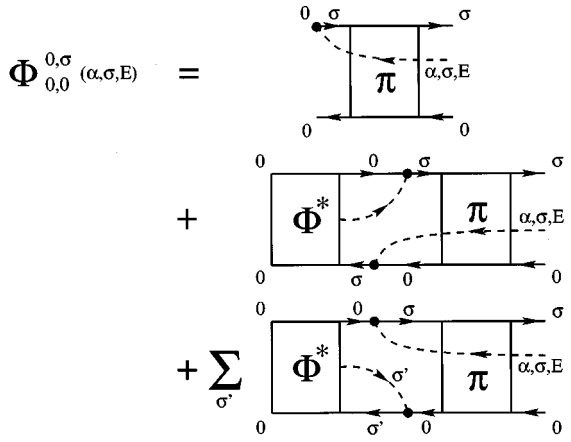


FIG. 8. Graphical representation of the self-consistent equation for $\phi$ beginning with an empty dot state.

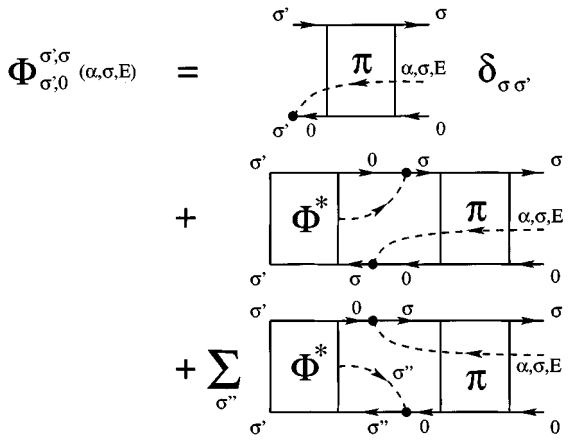

FIG. 9. Graphical representation of the self-consistent equation for $\phi$ beginning with an occupied dot state.

tunneling and boson lines. As pointed out in Appendix C, any approximation for $\phi$ will lead to a current conserving theory.

We construct the diagram $\phi$ by iteration (see Figs. 8 and 9). To do so, we need the diagram $\pi(E)$, which is the propagator, while a tunneling line with energy $E$ is running in parallel from the right to the left. This diagram can also be expressed as an iteration in the style of a Dyson equation (see Fig. 10)

$$\pi^{\chi_1',\chi_1}_{\chi_2',\chi_2}(E)=\pi^{(0)\chi_1'}_{\chi_2'}(E)\,\delta_{\chi_1',\chi_1}\delta_{\chi_2',\chi_2}+\sum_{\chi_1'',\chi_2''}\pi^{\chi_1',\chi_1''}_{\chi_2',\chi_2''}(E)\,\sigma^{\chi_1'',\chi_1}_{\chi_2'',\chi_2}(E)\,\pi^{(0)\chi_1}_{\chi_2}(E). \tag{45}$$

In analogy to $\Sigma$, the self-energy $\sigma(E)$ denotes the sum of all irreducible diagrams with a tunneling line going backward in time. Here the free propagator in energy space is given by

$$\pi^{(0)\chi_1}_{\chi_2}(E)=\frac{1}{E-(\epsilon_{\chi_1}-\epsilon_{\chi_2})+i0^+} \tag{46}$$

Hence we can solve Eq. (45) and find in matrix notation the general relation

$$\pi(E)=[[\pi^{(0)}(E)]^{-1}-\sigma(E)]^{-1}. \tag{47}$$

Because of the restriction to two charge states, only the matrix elements $\pi^{\sigma}(E)\equiv\pi^{\sigma,\sigma}_{0,0}(E)$ of $\pi(E)$ and $\sigma^{\sigma}(E)\equiv\sigma^{\sigma,\sigma}_{0,0}(E)$ of $\sigma(E)$ are involved, and we deduce from Eq. (47)

$$\pi^{\sigma}(E)=\frac{1}{E-\epsilon_{\sigma}-\sigma^{\sigma}(E)}. \tag{48}$$

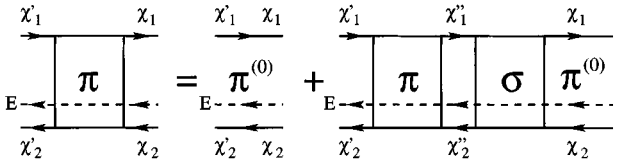

FIG. 10. Iteration of processes for the propagator $\pi$ with a tunneling line running in parallel from the right to the left.

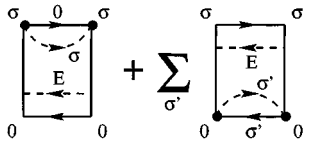

FIG. 11. In our approximation, the diagram for the irreducible self-energy $\sigma^{\sigma}(E)$ contains one tunneling line in addition to the backward running line.

Since at most two tunneling lines are allowed at once, the irreducible self-energy $\sigma^{\sigma}(E)$ consists of only one tunneling line. We calculate all contributions, that are depicted in Fig. 11, and get

$$\sigma^{\sigma}(E)=\int dE'\,\frac{\gamma^{-}(E')}{E-E'+i0^+}+\sum_{\sigma'}\int dE'\,\frac{\gamma^{+}(E')}{E-E'+\epsilon_{\sigma'}-\epsilon_{\sigma}+i0^+}. \tag{49}$$

In the spin degenerate case, this is exactly the relation (10) that we found from intuitive arguments.

According to our rules, Figs. 8 and 9 lead to the self-consistent equation for the diagram $\phi(\alpha,\sigma,E)$,

$$\phi^{0,\sigma}_{0,0}(\alpha,\sigma,E)=\pi^{\sigma}(E)\Bigg[\gamma^{+}_{\alpha}(E)-\gamma^{-}_{\alpha}(E)\sum_{\alpha'}\int dE'\times\frac{1}{E-E'+i0^+}\phi^{*0,\sigma}_{0,0}(\alpha',\sigma,E')-\gamma^{+}_{\alpha}(E)\sum_{\sigma'}\sum_{\alpha'}\int dE'\times\frac{1}{E-E'+\epsilon_{\sigma'}-\epsilon_{\sigma}+i0^+}\phi^{*0,\sigma'}_{0,0}(\alpha',\sigma',E')\Bigg] \tag{50}$$

and

$$\phi^{\sigma',\sigma}_{\sigma',0}(\alpha,\sigma,E)=\pi^{\sigma}(E)\Bigg[-\gamma^{-}_{\alpha}(E)\,\delta_{\sigma\sigma'}-\gamma^{-}_{\alpha}(E)\sum_{\alpha'}\int dE'\times\frac{1}{E-E'+i0^+}\phi^{*\sigma',\sigma}_{\sigma',0}(\alpha',\sigma,E')-\gamma^{+}_{\alpha}(E)\sum_{\sigma''}\sum_{\alpha'}\int dE'\times\frac{1}{E-E'+\epsilon_{\sigma''}-\epsilon_{\sigma}+i0^+}\times\phi^{*\sigma',\sigma''}_{\sigma',0}(\alpha',\sigma'',E')\Bigg]. \tag{51}$$

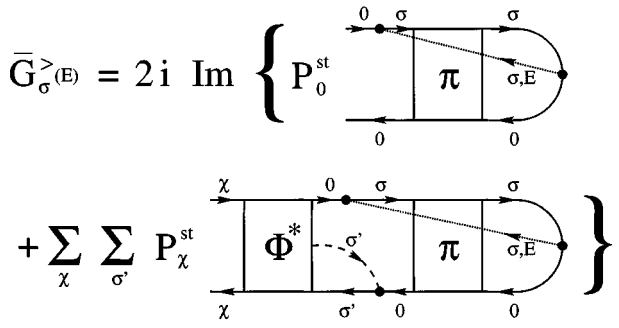


FIG. 12. Graphical representation of $\overline{G^{>}_{\sigma}}(E)$.

The stationary probabilities and the current are derived from Eqs. (29) and (36). To calculate the rates we specify Eq. (44) and obtain

$$\Sigma^{\alpha+}_{\chi',0} = 2i\ \mathrm{Im} \sum_{\sigma} \int dE\, \phi^{\chi',\sigma}_{\chi',0}(\alpha,\sigma,E), \tag{52}$$

$$\Sigma^{\alpha-}_{\chi',\sigma} = -2i\ \mathrm{Im} \int dE\, \phi^{\chi',\sigma}_{\chi',0}(\alpha,\sigma,E), \tag{53}$$

whereas all other rates are zero.

The correlation functions can be calculated from the diagrams shown in Figs. 12 and 13. We have to consider only the latest (i.e., rightmost) correlated part of the diagram. The processes before end up with probability $P^{st}_{\chi}$ in a diagonal state $\chi$. We have used the same criterion as for the calculation of the density matrix with one exception. If a vertical line lies between the external vertices, we allow a cut through at most one tunneling line. Here we have used the fact that such a vertical line will, in addition, always cut the virtual line connecting the external vertices. The sum of all these diagrams gives (where we can combine always two diagrams to the imaginary part of one of them)

$$G^{>}_{\sigma}(E) = \int dE'\, \overline{G^{>}_{\sigma}}(E') P^{+}(E'-E), \tag{54}$$

$$G^{<}_{\sigma}(E) = \int dE'\, \overline{G^{<}_{\sigma}}(E') P^{-}(E'-E), \tag{55}$$

with

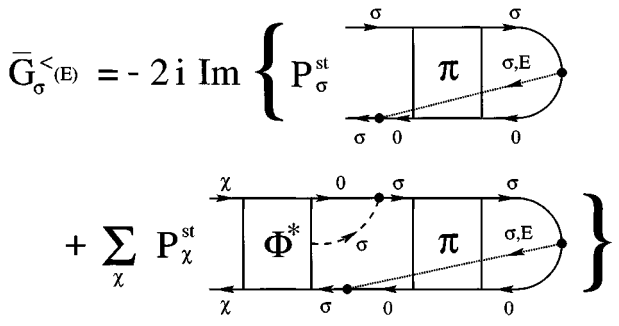


FIG. 13. Graphical representation of $\overline{G^{<}_{\sigma}}(E)$.

$$\overline{G^{>}_{\sigma}}(E) = 2i\ \mathrm{Im} \left\{ \pi^{\sigma}(E) \left[ P^{st}_0 - \sum_{\alpha}\sum_{\sigma'} \int dE' \times \frac{P^{st}_0 \phi^{*0,\sigma'}_{0,0}(\alpha,\sigma',E') + \sum_{\sigma''} P^{st}_{\sigma''} \phi^{*\sigma'',\sigma'}_{\sigma'',0}(\alpha,\sigma',E')}{E-E'+\epsilon_{\sigma'}-\epsilon_{\sigma}+i0^{+}} \right] \right\}, \tag{56}$$

$$\overline{G^{<}_{\sigma}}(E) = -2i\ \mathrm{Im} \left\{ \pi^{\sigma}(E) \left[ P^{st}_{\sigma} + \sum_{\alpha} \int dE' \times \frac{P^{st}_0 \phi^{*0,\sigma}_{0,0}(\alpha,\sigma,E') + \sum_{\sigma'} P^{st}_{\sigma'} \phi^{*\sigma',\sigma}_{\sigma',0}(\alpha,\sigma,E')}{E-E'+i0^{+}} \right] \right\}. \tag{57}$$

In the following, we discuss for transparency the effect of the coupling to bosons and the presence of a magnetic field separately.

### A. Boson-assisted tunneling

For zero magnetic field, i.e., $\epsilon_{\sigma}=\epsilon$ for all $\sigma$, we can perform the resummation of the corresponding diagrams for the rates and the Green's functions analytically (details are given in Appendix D) and find

$$I^{st}_{\alpha} = 2\pi e M \sum_{\alpha'} \int dE [\gamma^{-}_{\alpha}(E)\gamma^{+}_{\alpha'}(E) - \gamma^{-}_{\alpha'}(E)\gamma^{+}_{\alpha}(E)] |\pi(E)|^2, \tag{58}$$

with $\pi(E)=\pi^{\sigma}(E)$. We can write this equation in a more intuitive way by inserting the definition (7) for $\gamma^{\pm}_{\alpha}$,

$$I^{st}_{\alpha} = \frac{e}{h} \sum_{\alpha'} \int dE \int dE' \{ T_{\alpha',\alpha}(E',E) f_{\alpha'}(E') [1-f_{\alpha}(E)] - T_{\alpha,\alpha'}(E,E') f_{\alpha}(E) [1-f_{\alpha'}(E')] \}, \tag{59}$$

where

$$T_{\alpha,\alpha'}(E,E') = M \Gamma_{\alpha}(E) \Gamma_{\alpha'}(E') \times \int dE_1 P^{+}(E_1-E) P^{-}(E_1-E') |\pi(E_1)|^2 \tag{60}$$

can be interpreted as a transmission probability for an electron to start from reservoir $\alpha$ with energy $E$ and end in reservoir $\alpha'$ with energy $E'$. From the detailed balance condition (9) we get

$$T_{\alpha',\alpha}(E',E) = e^{\beta(E'-E)} T_{\alpha,\alpha'}(E,E'). \tag{61}$$

This guarantees that the current is zero if all chemical potentials of the reservoirs are identical.

However, the interpretation of $T_{\alpha,\alpha'}$ as a one-particle transmission probability in analogy to a generalization of the Landauer-Büttiker formula to inelastic interactions[51] is not correct. We see that the transmission probability still depends on the Fermi distribution functions via the self-energy $\sigma(E)$ in the denominator of the propagator $\pi(E)$. This reflects the many-particle aspect of the electron-electron and electron-boson interaction in our model.

Comparing our result for $T_{\alpha,\alpha'}$ with other approaches in the case $M=1$,[38–40,44] we see that the energy dependence of $\sigma(E)$ has been neglected in all previous treatments. We find that even in the $M=1$ case, the energy dependence of $\sigma(E)$ cannot been neglected if the temperature $T$ and the typical frequency $\omega_B$ of the bosons are smaller than $\Gamma$.

Without bosons, the current formula is exact up to order $\Gamma^2$, i.e., sequential and electron cotunneling are fully taken into account. With bosons, cotunneling is not described correctly since we have treated the bosons only by a dressing of the tunneling lines. This means that our approximation is not valid in regions where the current is very small. However, at resonance we believe our treatment to be correct since there we expect that sequential tunneling will be just modified by a renormalization and broadening of the local state of the dot that is described by the self-energy $\sigma(E)$, which is calculated in lowest order in $\Gamma$ here. Higher orders will be small for high tunneling barriers.

Finally, we calculate the Green's functions and find

$$G^{>}(E)=-2\pi i\int dE'\,\gamma^{-}(E')P^{+}(E'-E)|\pi(E')|^2, \tag{62}$$

$$G^{<}(E)=2\pi i\int dE'\,\gamma^{+}(E')P^{-}(E'-E)|\pi(E')|^2, \tag{63}$$

In equilibrium, i.e., $\mu_\alpha=0$ for all $\alpha$, we obtain the correct sum rule $G^{>}(E)=-\exp(\beta E)G^{<}(E)$. Furthermore, for the $M=1$ case, particle-hole symmetry is satisfied. The spectral density has the form

$$\rho(E)=\int dE'[\gamma^{+}(E')P^{-}(E'-E)+\gamma^{-}(E')P^{+}(E'-E)]|\pi(E')|^2. \tag{64}$$

The effect of the resonant-tunneling processes is described by the resolvent $\pi(E)$ containing the self-energy $\sigma(E)$ [Eq. (49)]. The real and imaginary parts of the self-energy express energy renormalization and broadening and determine, therefore, the position and the width of the maxima in the spectral density.

To proceed we consider from now on a one-mode environment (Einstein model) with boson frequency $\omega_q=\omega_B$. Experimentally realizations of this model are optical phonons[38–40] or by fluctuations of an external $LC$ circuit with frequency[41–44] $\omega_B=(LC)^{-1/2}$. The results for a general environment can be anticipated approximately from the one-mode case by a superposition. Furthermore, we choose the special case of two reservoirs $\alpha=L/R$ and constant level broadening $\Gamma/2=\Gamma_L=\Gamma_R$.

Defining $g=\Sigma_q g_q^2/\omega_B^2$ we obtain $P^{\pm}(E)=\Sigma_n p_n\delta(E\pm n\omega_B)$, where

$$p_n=e^{-g[1+2N_0(\omega_B)]}e^{n\omega_B/2T_B}I_n(2gN_0(\omega_B)e^{\omega_B/2T_B})$$

is the probability for the emission of $n$ bosons with frequency $\omega_B$. Here $N_0(\omega_B)$ is the Bose function and $I_n$ the modified Bessel function. Using Eq. (49) we obtain[15]

$$\mathrm{Re}\sigma(E)=\sum_{n,\alpha}(Mp_n-p_{-n})\frac{\Gamma_\alpha}{2\pi}\left[\ln\left(\frac{E_C}{2\pi T}\right)-\mathrm{Re}\Psi\left(\frac{1}{2}+i\frac{E+n\omega_B-\mu_\alpha}{2\pi T}\right)\right], \tag{65}$$

$$\mathrm{Im}\sigma(E)=-\pi\sum_n p_n[M\overline{\gamma^{+}}(E+n\omega_B)+\overline{\gamma^{-}}(E-n\omega_B)]. \tag{66}$$

Here $\Psi$ denotes the digamma function and we have chosen in the energy integrals a Lorentzian cutoff at $E_C$.

The real part of $\sigma(E)$ renormalizes the level position to higher energies. Furthermore, it depends logarithmically on energy, temperature, voltage, and frequency. These logarithmic terms are typical for the occurrence of Kondo peaks. Hence we anticipate logarithmic singularities either for $M\geqslant 2$ or for $p_n\neq p_{-n}$. This includes not only the degenerate case but also the case of a single dot level without spin ($M=1$) since the probabilities for absorption and emission of bosons are different. It is important to remark here that for systems coupled to classical time-dependent fields[22] the situation is different since then both probabilities are equal. At low enough temperatures we obtain logarithmic peaks in $\sigma(E)$ at $E=\mu_\alpha+n\omega_B$ ($n\neq 0$ for $M=1$). They lead to maxima of the resolvent $\pi(E)$ at $E=\mu_\alpha+n\omega_B$ ($n>0$ for $M=1$, $n\geqslant 0$ for $M>1$) for $\epsilon<0$ and at $E=\mu_\alpha+n\omega_B$ ($n<0$) for $\epsilon>0$. The spectral density (64) shows resonances at the same points but, due to the additional $P^{\pm}$ functions in the integrand, they are shifted by multiples of $\omega_B$. This boson-assisted tunneling is completely independent from the influence of the bosons on the self-energy $\sigma(E)$.

The spectral density at different voltages for a low-lying level $\epsilon<0$ is depicted in Fig. 14. Without an applied bias voltage, we obtain (for $M=2$) the usual Kondo peak near the Fermi level (which we choose as zero energy). The emission of bosons leads to additional resonances at multiples of $\omega_B$. For $M=1$ and $\epsilon<0$ resonances occur for negative energies, and in the case $\epsilon>0$, we find resonances at positive energies. In these cases, the effects are less pronounced and are only visible for very low temperatures. At finite bias voltages all peaks split and decrease in magnitude.

The resonances in the spectral density can be probed by the nonlinear differential conductance as a function of the bias voltage $V$, as shown in Fig. 15 for the case $\epsilon<0$. The splitting of the Kondo peak leads to an overall decrease of the spectral density in the energy range $|E|<eV$ (see the inset of Fig. 15). For this reason, the conductance shows the well-known[14,22,24] maximum at zero bias. The emission of bosons produces a set of symmetric satellite maxima. They can be traced back to the fact that pairs of Kondo peaks can merge if the bias voltage is a multiple of the boson frequency (see Fig. 14). This gives rise to pronounced Kondo peaks at

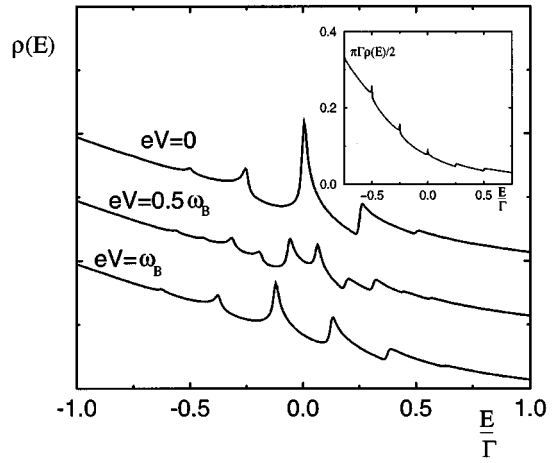


FIG. 14. Spectral density for $M=2$, $T=T_B=0.005\Gamma$, $\epsilon=-2\Gamma$, $g=0.2$, $\omega_B=0.25\Gamma$, and $E_C=50\Gamma$ at different voltages. For $V=0$ there are resonances at multiples of $\omega_B$, which split for finite bias voltage. Inset: spectral density for $M=1$, $T=0.000\,05\Gamma$, $T_B=0.5\Gamma$, $\epsilon=-\Gamma$, $V=0$, $g=0.5$, $\omega_B=0.25\Gamma$, and $E_C=50\Gamma$.

$E=\pm eV/2$ and thus to an increase of the spectral density with bias voltage near these points.

Figure 16 shows the differential conductance for $\epsilon \geqslant 0$ with and without bosons. A striking result is that the whole structure is inverted compared to the case $\epsilon<0$, and we find a zero-bias anomaly although the Kondo peak at zero energy is absent. The coupling to bosons yields satellite steps at $|eV|=n\omega_B$. The contributions of sequential and cotunneling lead, compared to resonant tunneling, only to a weak bias voltage dependence of the differential conductance. This shows clearly that the influence of the logarithmic terms in $\sigma(E)$ are still important. The logarithmic peaks in $\mathrm{Re}\sigma(E)$ decrease with increasing bias voltage and approach the value of $E-\epsilon$ if $\epsilon$ is large enough. Thus the value of $E-\epsilon-\mathrm{Re}\sigma(E)$ decreases, which in turn leads to an overall

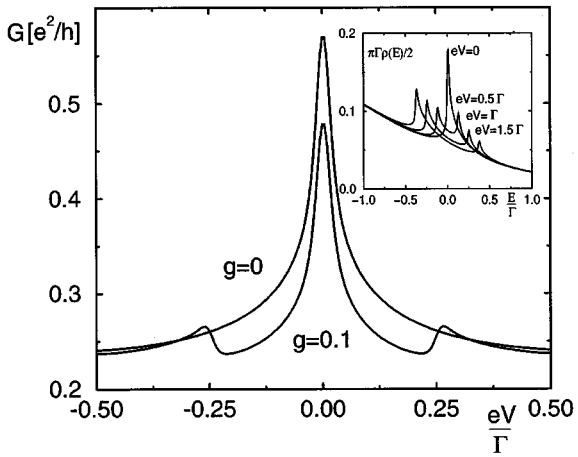


FIG. 15. Differential conductance vs bias voltage for $T=T_B=0.005\Gamma$, $\epsilon=-2\Gamma$, $\omega_B=0.25\Gamma$, and $E_C=50\Gamma$. The curves show a maximum at zero bias and satellite maxima at multiples of $\omega_B$ for a finite electron-boson coupling. Inset ($g=0$): increasing voltage leads to an overall decrease of the spectral density in the range $|E|<eV$.

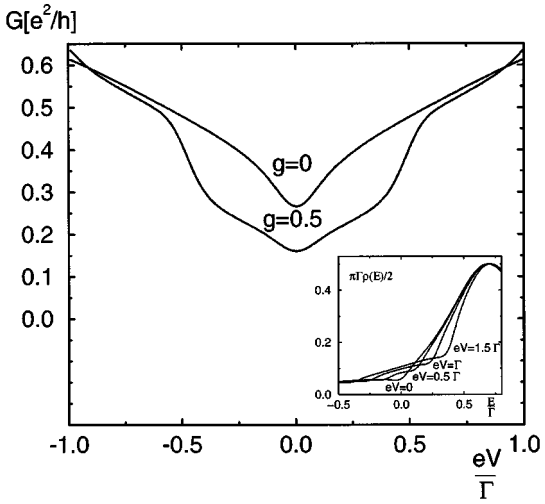


FIG. 16. Differential conductance vs bias voltage for $T=T_B=0.025\Gamma$, $\epsilon=0$, $\omega_B=0.5\Gamma$, and $E_C=50\Gamma$. The curves show a minimum at zero bias and steps at multiples of $\omega_B$ for a finite electron-boson coupling. Inset ($g=0$): increasing voltage leads to an overall increase of the spectral density in the range $|E|<eV$.

increase of the resolvent $\pi(E)$ and the spectral density $\rho(E)$ near zero energy (see the inset of Fig. 16).

Zero-bias minima are known from Kondo scattering from magnetic impurities.[52] They have been observed in recent experiments[53] and have been interpreted as two-channel Kondo scattering from atomic tunneling systems[54,49] or by tunneling into a disordered metal.[56] Here we have shown that zero-bias minima can also arise due to resonant tunneling via local impurities if the level position is high enough such that we are in the mixed valence regime.

Finally, we have investigated the differential conductance at fixed bias voltage as a function of the position of the dot level, which experimentally can be varied by a gate voltage coupled capacitively to the dot (see Fig. 17). The result shows a (classical) pair of peaks at $|\epsilon|=eV/2$ together with satellites (due to emission and absorption of bosons) and peaks for $|\epsilon|>eV/2$ (only due to absorption). The energy dependence of $\mathrm{Im}\sigma(E)$ gives rise to an asymmetry of the

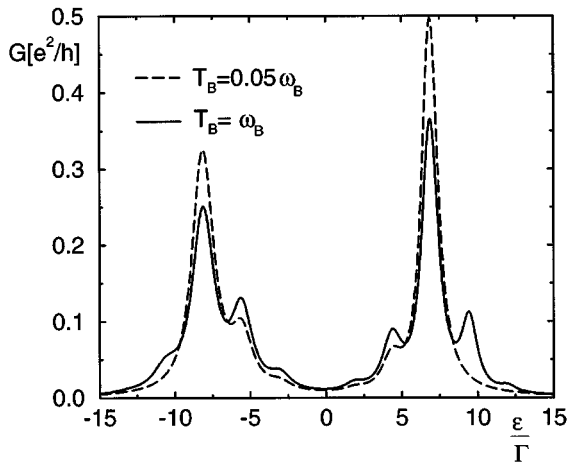


FIG. 17. Differential conductance as a function of $\epsilon$ for $T=0.125\Gamma$, $eV=15\Gamma$, $g=0.3$, $\omega_B=2.5\Gamma$, and $E_C=250\Gamma$.

peak heights. The peak at $\epsilon = eV/2$ is higher than the one at $\epsilon = -eV/2$ since $|\mathrm{Im}\sigma(E)| = \pi|M\gamma^+(E) + \gamma^-(E)|$ is smaller for higher energies (except for $M=1$ when particle-hole symmetry holds). This significant effect is due to the broadening of the spectral density by quantum fluctuations.

### B. Magnetic-field dependence

In this section we discuss the effect of an applied magnetic field and do not take into account the coupling to bosons. Again we consider the case of two reservoirs and constant level broadenings. Since the energy levels $\epsilon_\sigma$ are now spin dependent, we can no longer solve the self-consistent equations analytically but have to solve them numerically.

We find Kondo resonances in the spectral density $\rho_\sigma(E)$ at energies $E = \mu_\alpha + \epsilon_{\sigma'} - \epsilon_\sigma$ with $\sigma' \neq \sigma$. This is due to the fact that the correlation functions $G^<_\sigma(E)$ and $G^>_\sigma(E)$ are mainly determined by the resolvent $\pi^\sigma(E)$ [see Eqs. (56) and (57)], which contains, via the self-energy $\sigma^\sigma(E)$ logarithmic singularities at the corresponding energies,

$$\mathrm{Re}\sigma^\sigma(E) = \sum_\alpha \frac{\Gamma_\alpha}{2\pi} \sum_{\sigma' \neq \sigma} \left[ \ln\left(\frac{E_C}{2\pi T}\right) - \mathrm{Re}\Psi\left(\frac{1}{2} + i\frac{E + \epsilon_{\sigma'} - \epsilon_\sigma - \mu_\alpha}{2\pi T}\right)\right], \quad (67)$$

$$\mathrm{Im}\sigma^\sigma(E) = -\pi\left[\overline{\gamma^-}(E) + \sum_{\sigma'} \overline{\gamma^+}(E + \epsilon_{\sigma'} - \epsilon_\sigma)\right]. \quad (68)$$

From Eq. (42) we see that only energies within the window defined by the difference of the Fermi functions contribute to the current. For this reason, there is no Kondo-assisted tunneling at low transport voltage but sets on if transport voltage and level splitting are equal. Therefore, for low-lying levels the conductance peak at zero bias found in Sec. IV A now splits up into two peaks separated by the twice the level splitting[14] (see Fig. 18).

Ralph and Buhrman recently measured Kondo-assisted tunneling via a single-charge trap of a point contact tunnel barrier.[24] We follow the model proposed by the authors interpretating the experiment as a realization of the Anderson model with strong Coulomb repulsion such that double occupancy does not occur. However, we think that the interaction energy $U$ and not the conduction bandwidth is the relevant cutoff in this situation.

A comparison of the experiment and our theory is given in Figs. 18, 19, and 20. We find good agreement for the peaks induced by Kondo-assisted tunneling processes if we set the cutoff $U = 30$ meV. The authors suspect the single-charge trap to be a dangling bond, for which they expect $U = 100$ meV. Our result agrees in the order of magnitude; it gives a hint, however, that the state may have a larger extension than an ordinary dangling bond or that there is screening due to the copper electrodes or both. The peaks for larger magnetic fields show, however, a stronger broadening than predicted from our calculation. Nevertheless, our theory reproduces the experimental curves much better than the fits given in Ref. 24 using perturbation theory since we have taken into account nonperturbative effects, which are obviously important here.

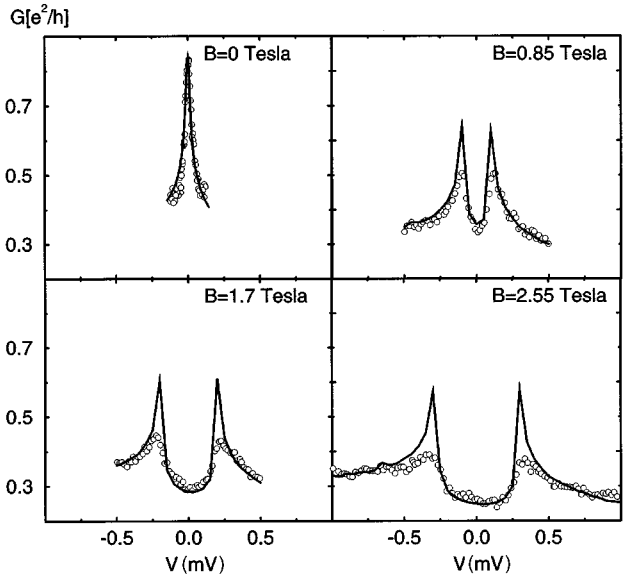


FIG. 18. Differential conductance vs bias voltage for $T = 4.3$ $\mu$eV, $\epsilon_\sigma(B=0) = -5.2$ meV, $\Gamma = 3.4$ meV, $a_c = 0.33$, and $E_C = 30$ meV. The circles are experimental data from Ref. 24.

The model proposed by the authors of Ref. 24 explains the broad peaks at large voltages by the matching of the energies of the empty and the singly occupied dot. Our calculations for this case, however, lead to a broader and lower peak for positive voltages in comparison with experiment (see Fig. 19). We think, therefore, that due to the capacitance asymmetry the system becomes doubly occupied before the empty state is energetically favorable. The capacitance asymmetry $a_c$ makes then the corresponding resonance peak sharper. An energy-dependent transparency of the barriers could then explain the different heights. A generalization of our theory to situations, where multiple occupancy of the dot is important, is currently under way and will be presented elsewhere.

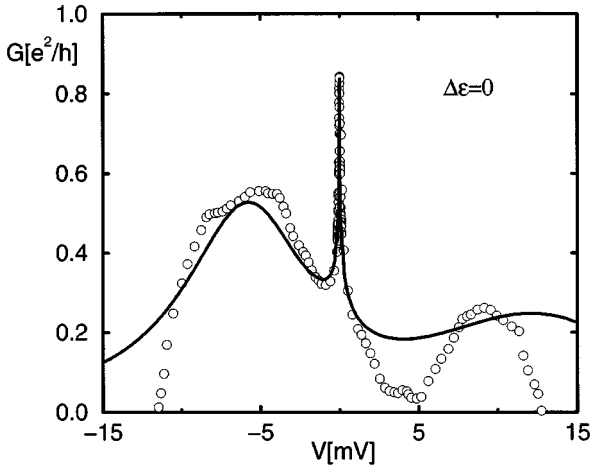


FIG. 19. Differential conductance vs bias voltage for $T = 4.3$ $\mu$eV, $\epsilon_\sigma = -5.2$ meV, $B = 0$, $\Gamma = 3.4$ meV, $a_c = 0.33$, and $E_C = 30$ meV. The circles are experimental data from Ref. 24.

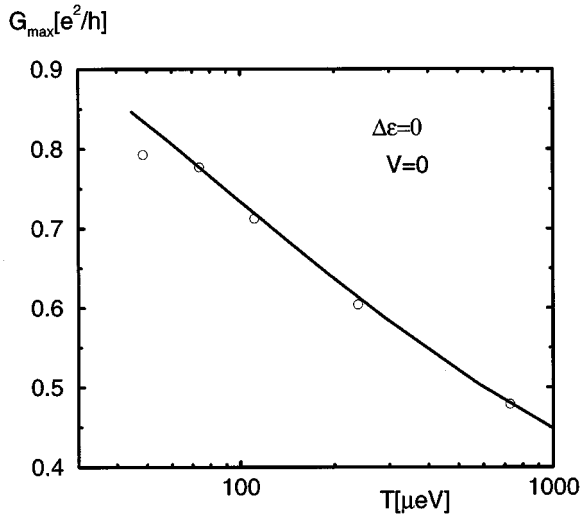


FIG. 20. Maximal linear conductance vs temperature for $\epsilon_\sigma = -5.2$ meV, $B=0$, $\Gamma=3.4$ meV, $a_c=0.33$, and $E_C=30$ meV. The circles are experimental data from Ref. 24.

Finally, we consider the case when the energy level is above the Fermi energies of the leads. The zero-bias minimum found in Sec. IV A splits for finite magnetic field into two minima separated by twice the level splitting (see Fig. 21).

## V. CONCLUSION

In conclusion, we have studied low-temperature transport in the nonequilibrium Anderson model with bosonic interactions. The latter yield Kondo resonances in the spectral density that can be probed by the measurement of the nonlinear differential conductance. Both the gate and bias voltage dependence are important. Quantum fluctuations due to resonant tunneling yield zero-bias anomalies as a function of the bias voltage, *which can be changed from maxima to minima by varying the gate voltage*. Furthermore, we discussed the splitting of the zero-bias anomaly by an external magnetic field and found good agreement with recent experiments.

We have presented a real-time approach that is based on a nonperturbative calculation of transition rates between different states of a local strongly correlated system coupled to fermionic or bosonic baths. We present systematic rules of how to set up well-defined perturbation expansions for the rates in terms of the tunneling matrix elements between dot and leads. The formally exact rates are used to calculate occupation probabilities and the current from master equations and current formulas that are intuitively obvious. The method has a wide applicability, ranging from the study of arbitrary dot level structures to the investigation of macroscopic quantum coherence phenomena. The latter can arise from the time evolution of nonstationary initial states or by the application of explicitly time-dependent fields.

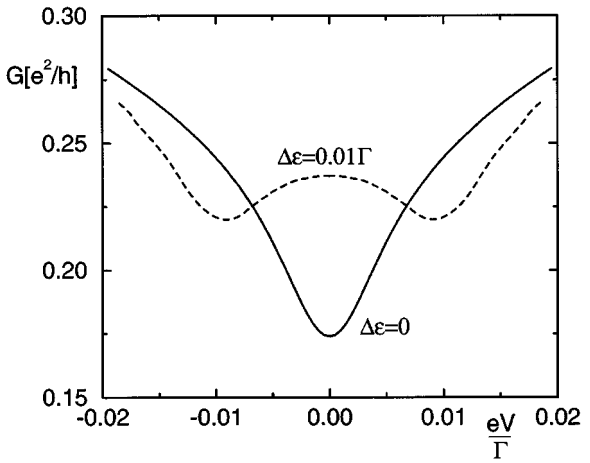


FIG. 21. Differential conductance vs bias voltage for $T=0.001\Gamma$, $\epsilon_\sigma=0.1\Gamma\pm\Delta\epsilon/2$, and $E_C=10\Gamma$.

The usage of real-time methods to understand low-temperature behavior of strongly correlated fermions in either equilibrium or nonequilibrium situations is a rather new field and has not yet been extensively applied. Compared with the conventional methods in imaginary time,[55] they offer the possibility to set up new approximation schemes. In this paper we have performed a nonperturbative resummation of higher-order coherent tunneling processes to calculate transition and current rates analytically for temperatures smaller than the intrinsic broadening $\Gamma$. Although the criterion for considering certain diagrams is yet not motivated by the usage of a ''small'' parameter, the diagrams are selected in a systematic way. We have chosen all diagrams that keep the total density matrix as close as possible to the diagonal state up to one electron-hole pair excitation in the reservoirs. This is reminiscent of the technique applied within a variational wave function Ansatz[58] but here formulated on the basis of density matrices for nonequilibrium systems at finite temperatures. Furthermore, there are many possibilities to improve our approximation by considering more diagrams by analytical or numerical methods. Simple limiting cases as, e.g., the noninteracting case are already exactly incorporated within our approximation. Since the strongly interacting case gives also at least qualitatively good results, our method may be a good candidate to cover the whole range from weak to strong interaction within the same approximation scheme.

## ACKNOWLEDGMENTS

We like to thank D. Averin, J. von Delft, and M. Hettler for useful discussions. The support by the Deutsche Forschungsgemeinschaft, through Sonderforschungsbereich 195, by the Swiss National Science Foundation (H.S.), and by the Academy of Finland (G.S.) is gratefully acknowledged.

## APPENDIX A: RULES IN TIME SPACE

Each term of the expansion Eq. (17) with operators $A_i$ of the form Eq. (18) can be calculated according to the following rules.

(1) Draw all topological different diagrams with directed tunneling lines connecting pairs of internal or external vertices containing lead electron operators. Assign a reservoir index $\alpha$ and a spin index $\sigma$ to each of these lines. Connect all vertices containing boson operators in all possible ways by boson lines. Assign states $\chi$ and the corresponding energy $\epsilon_\chi$ to each element of the Keldysh contour connecting two vertices.

(2) The propagation from $t'$ to $t$ with $t'<t$ on the Keldysh contour implies a factor $\exp[-i\epsilon_\chi(t-t')]$.

(3) The state $\chi$ that is assigned to the leftmost part of the diagram implies a factor $P^0_\chi$ from the initial density matrix. Each vertex containing a dot operator $B$ gives rise to a matrix element $\langle\chi'|B|\chi\rangle$, where $\chi$ ($\chi'$) is the dot state entering (leaving) the vertex with respect to the Keldysh contour.

(4) Each directed tunneling line with index $\alpha$ running from $t'$ to $t$ implies $(-1)^v\overline{\gamma^K_\alpha}(t,t')$, with $v$ being the number of electron operators (due to external vertices) on the part of the Keldysh contour from $t'$ to $t$. The line corresponds to a tunneling process in reservoir $\alpha$. Each boson line connecting vertices at times $t$ and $t'$ implies $P^K(t,t')$ if the phase factors at these vertices have different sign. Otherwise, the boson line has the value $P^K(t,t')^{-1}$.

(5) Each diagram carries a prefactor $(-i)^m(-1)^c$, where $m$ is the total number of internal vertices and $c$ the number of crossings of tunneling lines. There may be another minus sign due to the order of dot electron operators, which emerges from the matrix elements $\langle\chi'|B|\chi\rangle$ discussed in rule 3.

(6) Integrate over the internal times along the Keldysh contour without changing their ordering and sum over the reservoir and spin indices.

We emphasize that these diagrammatic rules hold for arbitrary dot Hamiltonians $H_D=\Sigma_\chi\epsilon_\chi|\chi\rangle\langle\chi|$, i.e., the states $\chi$ can be many-body eigenfunctions of $H_D$ containing complicated correlations due to Coulomb interaction, magnetic fields, geometric setups, etc. Such eigenfunctions have been calculated for special situations[59,60] and can be used as an input for our diagrammatic language. In this paper, however, we will concentrate ourselves on the dot Hamiltonian (5), where the states $\chi$ are trivially known. For this special case, the matrix elements $\langle\chi'|B|\chi\rangle$ from rule 3 can only give rise to minus signs, whereas they can have a more pronounced influence in more general situations.[59,60]

Furthermore, we note that the same diagrammatic rules even hold for arbitrary time-dependent dot Hamiltonians $H_D(t)$ that are not diagonal in the states $\chi$. In this case one has to assign two states $\chi'$ and $\chi$ to the beginning and the end of each element of the Keldysh contour, respectively. The factor $\exp[-i\epsilon_\chi(t-t')]$ from rule 2 is then replaced by the matrix element $\langle\chi|U_D(t,t')|\chi'\rangle$, where $U_D$ denotes the time evolution operator of $H_D$ and $t$ ($t'$) are the times at the end (beginning) of the element of the Keldysh contour.

## APPENDIX B: RULES IN ENERGY SPACE

We obtain the diagrammatic rules in energy space by expanding the expectation value in Eq. (21) and then performing the time integrals. We order the times of all internal ($m$) and external vertices ($n$) from left to right and label them by $\tau_j$ with $j=1,2,\ldots,m+n$ (with $\tau_{m+n}=0$), irrespective on which branch they are. The Keldysh contour integrals are now written as ordinary integrals. This includes a minus sign for each internal vertex on the backward propagator. If the initial density matrix is diagonal we then encounter expressions of the type

$$\int_{-\infty}^{0}d\tau_1\int_{\tau_1}^{0}d\tau_2\cdots\int_{\tau_{m+n-2}}^{0}d\tau_{m+n-1}e^{0^+\tau_1}e^{-i\Delta E_1(\tau_1-\tau_2)}\times e^{-i\Delta E_2(\tau_2-\tau_3)}\cdots e^{-i\Delta E_{m+n-1}\tau_{m+n-1}}=i^{m+n-1}\frac{1}{\Delta E_1+i0^+}\frac{1}{\Delta E_2+i0^+}\cdots\frac{1}{\Delta E_{m+n-1}+i0^+}. \tag{B1}$$

Here $\Delta E_j$ is the difference of all energies going to the left minus, all energies going to the right in each segment limited by $\tau_j$ and $\tau_{j+1}$. This includes the energies of the propagators and, if present, the energies of the tunneling, boson, and virtual lines. The convergence factor $e^{0^+\tau_1}$ is related to an adiabatic switching on of the tunneling term $H_T$. The factor $i^{m+n-1}$ cancels with the factor $(-i)^m$ from rule 4 above together with the prefactor $(-i)^{n-1}$ from the definition Eq. (B1). Therefore, the corresponding rules in energy representation read as follows.

(1′) Draw all topologically different diagrams with fixed ordering of the vertices along the real axis, i.e., irrespective on which branch they are. The vertices are connected by tunneling and boson lines as in time space. In addition to the energy $\epsilon_\chi$ assigned to the propagators we assign an energy $E$ to each tunneling line. For each boson line choose a direction (arbitrarily) and assign also an energy $E$. The external vertices are connected by virtual lines with energies $E_i$ ($i=2,\ldots,n$) as described above.

(2′) For each segment derived from $\tau_j\leqslant\tau\leqslant\tau_{j+1}$ with $j=1,2,\ldots,m+n-1$ assign a resolvent $1/(\Delta E_j+i0^+)$, where $\Delta E_j$ is the difference of the leftgoing energy minus the rightgoing energy (including the energies of the tunneling, boson, and virtual lines).

(3′) See rule 3 in time space.

(4′) For each coupling of vertices write $(-1)^v\overline{\gamma^+_\alpha}(E)$ if the tunneling line of reservoir $\alpha$ is going backward and $(-1)^v\overline{\gamma^-_\alpha}(E)$ if it is going forward with respect to the closed time path (definition of $v$ see rule 4 in time space). For each boson line write $P^+(E)$ if it is going backward and $P^-(E)$ if it is going forward with respect to the closed time path.

(5′) The prefactor is given by $(-1)^b(-1)^c$, where $b$ is the total number of internal vertices on the backward propagator and $c$ the number of crossings of tunneling lines. There may be another minus sign due to the order of dot electron operators that emerges from the matrix elements $\langle\chi'|B|\chi\rangle$ discussed in rule 3.

(6′) Integrate over the energies of tunneling and boson lines and sum over the reservoir and spin indices.

## APPENDIX C: CURRENT CONSERVATION

In this appendix we prove Eq. (34) and current conservation. Let us consider any diagram $\Sigma^{\alpha p}_{\chi',\chi}(t',t)$ in the expression

$$\sum_\chi\sum_p p\Sigma^{\alpha p}_{\chi',\chi}(t',t). \tag{C1}$$

By changing the vertical position of the rightmost vertex we get a new diagram that has up to a minus sign the same value as the old diagram from which the new one was constructed. If the rightmost tunneling of the old diagram line has a reservoir index different from $\alpha$, then the new diagram is of the form $\Sigma^{\alpha p}_{\chi',\chi''}$, so that the sum of all these contributions in Eq. (C1) is zero. The other diagrams are divided into two classes: in one (the other) class, the rightmost tunneling line of each diagram enters (leaves) the forward propagator or leaves (enters) the backward propagator. The change of the vertical position of the rightmost vertex then increases (decreases) the value of $p$ by one, so that the new diagram is of the form $\Sigma^{\alpha p\pm 1}_{\chi',\chi''}$. Furthermore, the old and the new diagram belong to different classes. After changing the position of the rightmost vertex of only one class and then shifting the summation index $p$ in Eq. (C1), we obtain exactly all diagrams of $\Sigma_\chi \Sigma^{\alpha+}_{\chi',\chi}$, which proves Eq. (34).

The conservation of probability follows directly from the master equation (26). Summation over $\chi$ together with $\Sigma_\chi \Sigma_{\chi',\chi}(t',t)=0$ yields

$$\sum_\chi \frac{d}{dt} P_\chi(t)=0\,. \tag{C2}$$

To prove current or charge conservation we first recognize that

$$\sum_{\substack{\chi\\ N(\chi)=p}} \Sigma^{\alpha+}_{\chi',\chi} = -\sum_{\substack{\chi\\ N(\chi)=p+1}} \Sigma^{\alpha-}_{\chi',\chi}, \tag{C3}$$

where $N(\chi)$ is the particle number on the dot for state $\chi$. This relation follows directly by changing the vertical position of the rightmost vertex.

After multiplication of the master equation (26) with $-e$ and $N(\chi)$ and summation over $\chi$, we use Eqs. (33) and (C3), insert the current formula (32), and find the conservation law for the total charge flowing into the dot

$$\sum_\alpha I_\alpha(t)=\frac{d}{dt}Q(t), \tag{C4}$$

where $Q=-eN=-e\Sigma_\chi N(\chi)P_\chi$ is the charge on the dot. In the stationary and time-independent case Eq. (C4) reduces to the conservation of the tunneling current

$$\sum_\alpha I^{\rm st}_\alpha=0, \tag{C5}$$

whereas for the general case the right-hand side of Eq. (C4) is minus the sum over all displacement currents flowing in the reservoirs.

An important result of this appendix is that any approximation for the rates is current conserving provided that the condition Eq. (C3) is satisfied. This means that we always have to consider both vertical positions of the rightmost vertex.

## APPENDIX D: ANALYTIC SOLUTION FOR ZERO MAGNETIC FIELD

For zero magnetic field, i.e., $\epsilon_\sigma=\epsilon$ for all $\sigma$, we define the quantities $\pi(E)\equiv\pi^\sigma(E)$, $\sigma(E)\equiv\sigma^\sigma(E)$, and

$$\phi^+_\alpha(E)=\phi^{0,\sigma}_{0,0}(\alpha,\sigma,E), \quad \phi^-_\alpha(E)=\sum_{\sigma'}\phi^{\sigma,\sigma'}_{\sigma,0}(\alpha,\sigma',E), \tag{D1}$$

which are independent of $\sigma$. We get the integral equations

$$[E-\epsilon-\sigma(E)]\phi^\pm_\alpha(E)=\pm\gamma^\pm_\alpha(E)-\gamma_\alpha(E)\int dE' \times\frac{1}{E-E'+i0^+}\phi^{*\pm}(E'), \tag{D2}$$

where $\gamma_\alpha(E)=\gamma^-_\alpha(E)+M\gamma^+_\alpha(E)$ and $\phi^\pm(E)=\Sigma_\alpha\phi^\pm_\alpha(E)$. Summing over $\alpha$ and taking the imaginary part, we obtain the solution

$$\mathrm{Im}\phi^\pm(E)=\mp\pi\frac{\lambda^\pm}{\lambda}\gamma(E)|\pi(E)|^2, \tag{D3}$$

where we used the definitions $\gamma^\pm(E)=\Sigma_\alpha\gamma^\pm_\alpha(E)$, $\gamma(E)=\gamma^-(E)+M\gamma^+(E)$,

$$\lambda^\pm=\int dE\,\gamma^\pm(E)|\pi(E)|^2, \quad \lambda=\int dE|\pi(E)|^2. \tag{D4}$$

Furthermore, we obtain directly from (D2) a relation between $\phi_\alpha$ and $\phi$,

$$\gamma(E)\phi^\pm_\alpha(E)=\gamma_\alpha(E)\phi^\pm(E) \pm\pi(E)[\gamma(E)\gamma^\pm_\alpha(E)-\gamma^\pm(E)\gamma_\alpha(E)]. \tag{D5}$$

Using (52), the current rates follow from $\Sigma^{\alpha+}_{0,0}=2iM\int dE\ \mathrm{Im}\phi^+_\alpha(E)$ and $\Sigma^{\alpha+}_{\sigma,0}=2i\int dE\ \mathrm{Im}\phi^-_\alpha(E)$. With Eqs. (D3) and (D5), the result is

$$\Sigma^{\alpha+}_{0,0}=-2\pi iM\left[\frac{\lambda^+}{\lambda}\lambda_\alpha+\int dE|\pi(E)|^2 \times[\gamma^-(E)\gamma^+_\alpha(E)-\gamma^+(E)\gamma^-_\alpha(E)]\right], \tag{D6}$$

$$\Sigma^{\alpha+}_{\sigma,0}=2\pi i\left[\frac{\lambda^-}{\lambda}\lambda_\alpha-M\int dE|\pi(E)|^2 \times[\gamma^-(E)\gamma^+_\alpha(E)-\gamma^+(E)\gamma^-_\alpha(E)]\right], \tag{D7}$$

where $\lambda_\alpha=\int dE\,\gamma_\alpha(E)|\pi(E)|^2$.

Summing the current rates over $\alpha$ and using $\Sigma_\alpha \lambda_\alpha = \lambda^- + M\lambda^+ = 1$, we get the total transition rates (note that $\Sigma^{\alpha-}_{\chi',0} = 0$)

$$\Sigma_{0,0} = -2\pi i M \frac{\lambda^+}{\lambda}, \quad \Sigma_{\sigma,0} = 2\pi i \frac{\lambda^-}{\lambda} \tag{D8}$$

and the solution of the stationary master equation (29) reads

$$P_0^{\rm st} = \lambda^-, \quad P_\sigma^{\rm st} = \lambda^+ \quad \text{with } \lambda^- + M\lambda^+ = 1. \tag{D9}$$

The stationary current follows from (36) $I_\alpha^{\rm st} = -ie[P_0^{\rm st}\Sigma^{\alpha+}_{0,0} + MP_\sigma^{\rm st}\Sigma^{\alpha+}_{\sigma,0}]$ (note that $\Sigma^{\alpha+}_{\chi',\sigma} = 0$), which gives as the final result Eq. (58).


[1] P.L. McEuen and L.P. Kouwenhoven, in *Nano-Science and Technology*, edited by G. Timp (AIP, New York, in press).

[2] B.Su.V.J. Goldman and J.E. Cunningham, Science **255**, 313 (1992).

[3] P. Gueret, N. Blanck, R. Germann, and H. Rothuizen, Phys. Rev. Lett. **68**, 1896 (1992).

[4] A.T. Johnson, L.P. Kouwenhoven, W. de Jong, N.C. van der Vaart, C.J.P.M. Harmans, and C.T. Foxon, Phys. Rev. Lett. **69**, 1592 (1992).

[5] E.B. Foxman, P.L. McEuen, U. Meirav, N.S. Wingreen, Y. Meir, P.A. Belk, N.R. Belk, M.A. Kastner, and S.J. Wind, Phys. Rev. B **47**, 10 020 (1993).

[6] J. Weis, R.J. Haug, K. von Klitzing, and K. Ploog, Phys. Rev. B **46**, 12 837 (1992).

[7] D.C. Ralph, C.T. Black, and M. Tinkham, Phys. Rev. Lett. **74**, 3241 (1995).

[8] D.V. Averin, A.N. Korotkov, and K.K. Likharev, Phys. Rev. B **44**, 6199 (1991).

[9] C.W.J. Beenakker, Phys. Rev. B **44**, 1646 (1991).

[10] D. Weinmann, W. Häusler, W. Pfaff, B. Kramer, and U. Weiss, Europhys. Lett. **26**, 467 (1994).

[11] C. Bruder and H. Schoeller, Phys. Rev. Lett. **72**, 1076 (1994).

[12] L.I. Glazman and K.A. Matveev, Pis'ma Zh. Éksp. Teor. Fiz. **48**, 403 (1988) [JETP Lett. **48**, 445 (1988)].

[13] S. Hershfield, J.H. Davies, and J.W. Wilkins, Phys. Rev. Lett. **67**, 3720 (1991); Phys. Rev. B **46**, 7046 (1992).

[14] Y. Meir, N.S. Wingreen, and P.A. Lee, Phys. Rev. Lett. **70**, 2601 (1993); N.S. Wingreen and Y. Meir, Phys. Rev. B **49**, 11 040 (1994).

[15] J. König, H. Schoeller, and G. Schön, Phys. Rev. Lett. **76**, 1715 (1996); in *Festkörperprobleme: Advances in Solid State Physics*, edited by R. Helbig (Vieweg, Braunschweig, 1996), Vol. 35, p. 215.

[16] A. Groshev, T. Ivanov, and V. Valtchinov, Phys. Rev. Lett. **66**, 1082 (1991).

[17] T.K. Ng and P.A. Lee, Phys. Rev. Lett. **61**, 1768 (1988).

[18] L.I. Glazman and M.E. Raikh, Pis'ma Zh. Éksp. Teor. Fiz. **47**, 378 (1988) [JETP Lett. **47**, 452 (1988)].

[19] A. Kawabata, J. Phys. Soc. Jpn. **60**, 3222 (1991).

[20] T.K. Ng, Phys. Rev. Lett. **70**, 3635 (1993).

[21] A.L. Yeyati, A. Martin-Rodero, and F. Flores, Phys. Rev. Lett. **71**, 2991 (1993).

[22] M.H. Hettler and H. Schoeller, Phys. Rev. Lett. **74**, 4907 (1995).

[23] C. Bruder, R. Fazio, and H. Schoeller, Phys. Rev. Lett. **76**, 114 (1996).

[24] D.C. Ralph and R.A. Buhrman, Phys. Rev. Lett. **72**, 3401 (1994).

[25] N.E. Bickers, Rev. Mod. Phys. **59**, 845 (1987).

[26] F.D.M. Haldane, Phys. Rev. Lett. **40**, 416 (1978).

[27] R.P. Feynman and F.L. Vernon, Ann. Phys. (N.Y.) **24**, 118 (1963).

[28] A. O. Caldeira and A. J. Leggett, Physica A **121**, 587 (1983).

[29] U. Weiss, *Quantum Dissipative Systems* (World Scientific, Singapore, 1993), Vol. 2.

[30] U. Eckern, G. Schön, and V. Ambegaokar, Phys. Rev. B **30**, 6419 (1984).

[31] G. Schön and A.D. Zaikin, Phys. Rep. **198**, 237 (1990).

[32] G. Schön, in *Quantum Processes and Dissipation*, edited by B. Kramer *et al.* (VCH, Weinheim, in press), Chap. 4.

[33] H. Schoeller and G. Schön, Phys. Rev. B **50**, 18 436 (1994); Physica B **203**, 423 (1994).

[34] J. König, H. Schoeller, and G. Schön, Europhys. Lett. **31**, 31 (1995); in *Quantum Dynamics of Submicron Structures*, Vol. 291 of *NATO Advanced Study Institute, Series E: Applied Science*, edited by H. A. Cerdeira *et al.* (Kluwer, Dordrecht, 1995), p. 221.

[35] J. Stampe and H. Schoeller (unpublished).

[36] A.E.A. Koolen, Diploma thesis, Technische Universiteit Delft, 1996.

[37] T.K. Ng, Phys. Rev. Lett. **76**, 487 (1996).

[38] N.S. Wingreen, K.W. Jacobsen, and J.W. Wilkins, Phys. Rev. Lett. **61**, 1396 (1988); Phys. Rev. B **40**, 11 834 (1989).

[39] L.I. Glazman and R.I. Shekhter, Zh. Éksp. Teor. Fiz. **94**, 292 (1988) [Sov. Phys. JETP **67**, 163 (1988)].

[40] M. Jonson, Phys. Rev. B **39**, 5924 (1989).

[41] M.H. Devoret, D. Esteve, H. Grabert, G.-L. Ingold, H. Pothier, and C. Urbina, Phys. Rev. Lett. **64**, 1824 (1990).

[42] A.A. Odintsov, G. Falci, and G. Schön, Phys. Rev. B **44**, 13 089 (1991).

[43] K. Flensberg, S.M. Girvin, M. Jonson, D.R. Penn, and M.D. Stiles, Phys. Scr. **T42**, 189 (1992).

[44] H.T. Imam, V.V. Ponomarenko, and D.V. Averin, Phys. Rev. B **50**, 18 288 (1994).

[45] A.O. Caldeira and A.J. Leggett, Ann. Phys. (N.Y.) **149**, 374 (1983); **153**, 445(E) (1983).

[46] G.D. Mahan, *Many-Particle Physics* (Plenum, New York, 1990).

[47] G. Ingold and Yu.V. Nazarov, in *Single Charge Tunneling*, 1992 Les Houches Lectures, edited by H. Grabert and M. Devoret (Plenum, New York, 1992).

[48] M. Grifoni, M. Sassetti, and U. Weiss, Phys. Rev. E **53**, R2033 (1996).

[49] M.H. Hettler, J. Kroha, and S. Hershfield, Phys. Rev. Lett. **73**, 1967 (1994).

[50] C. Caroli, R. Combescot, P. Nozières, and D. Saint-James, J. Phys. C **5**, 21 (1972).

[51] F. Hekking, Y.V. Nazarov, and G. Schön, Europhys. Lett. **14**, 489 (1991); **20**, 255 (1992).

[52] A.G.M. Jansen, A.P. van Gelder, P. Wyder, and S. Strassler, J. Phys. F **11**, L15 (1981).

[53] D.C. Ralph and R.A. Buhrman, Phys. Rev. Lett. **69**, 2118 (1992); Phys. Rev. B **51**, 3554 (1995).

[54] D.C. Ralph, A.W.W. Ludwig, J. von Delft, and R.A. Buhrman, Phys. Rev. Lett. **72**, 1064 (1994); **75**, 770 (1995); **75**, 2786 (1995).
[55] H. Keiter and G. Morandi, Phys. Rep. **109**, 227 (1984).
[56] N.S. Wingreen, B.L. Altshuler, and Y. Meir, Phys. Rev. Lett. **75**, 769 (1995).
[57] H. Schoeller, Habilitationsschrift, Universität Karlsruhe, 1996.
[58] O. Gunnarsson and K. Schönhammer, Phys. Rev. Lett. **50**, 604 (1983); Phys. Rev. **28**, 4315 (1983).
[59] D. Pfannkuche and S.E. Ulloa, Phys. Rev. Lett. **74**, 1194 (1995).
[60] K. Jauregui, W. Häusler, D. Weinmann, and B. Kramer, Phys. Rev. B **53**, R1713 (1996).